Far Western analysis was carried out as described below. Each fraction separated by discontinuous sucrose density gradient centrifugation was subjected to SDS-PAGE. After electrophoresis, proteins were transferred onto a nitrocellulose membrane, which was incubated for 2 h at room temperature in 3× PBS containing 1% blocking reagent (Roche Applied Science). The membrane was further incubated overnight at room temperature with 0.02% (v/v) of HrVC70 in 3× PBS containing 0.1% SDS and 3% blocking reagent. HrVC70-interacting protein band(s) were detected by anti-HrVC70 rabbit antibody using the ECL system (Amersham Biosciences).

Inhibitory ability of anti-HrUrabin antibody on this interaction was examined by adding anti-HrUrabin antibody during incubation with HrVC70. To distinguish two rabbit antibodies (anti-HrVC70 and anti-HrUrabin), biotin-labeled anti-HrVC70 antibody and horseradish peroxidase-conjugated streptavidin (Calbiochem) were used to detect the HrVC70-interacting protein(s) on a membrane.

For immunocytochemistry, spermatozoa supported on the aminopropyltriethoxysilane-coated slide glass (Matsunami Glass) were fixed with 4% paraformaldehyde in 1× PBS for 1 h at room temperature. After several washes with 1× PBS, the specimen was reacted with 1/1000 diluted anti-HrUrabin antiserum in 1× PBS containing 1% bovine serum albumin for 1 h at room temperature, then washed several times, followed by incubation with 2 μg/ml of Alexa Fluor 568 goat anti-rabbit IgG antibody (Invitrogen) and 5 μg/ml of 4′,6-diamino-2-phenylindole (Sigma) in 1× PBS for 1 h at room temperature. After washing with 1× PBS, the specimen was observed under an inverted fluorescent microscope (Nikon).

Enzymatic Elimination Procedures of GPI Anchor and Sugar Chains—To examine whether HrUrabins are sperm-surface GPI-anchored proteins, intact sperm was incubated with 1 unit of phosphatidylinositol-specific phospholipase C (PI-PLC, Sigma) for 1 h at 37 °C, followed by centrifugation at 15,000 × *g* for 10 min. The obtained supernatant was subjected to Western analysis using the anti-HrUrabin antibody.

An *N*-linked glycosylation site on each HrUrabin species was predicted from their amino acid sequences. To examine whether a carbohydrate chain is linked to the consensus Asn residue of HrUrabins, the LD-DIM fraction was incubated with 5 units of PNGase F (Sigma) in 50 mM phosphate buffer (pH 8.0) for 2 h at 37 °C. The reacted sample was subjected to SDS-PAGE, followed by Western and Far Western analyses.

Amino Acid Sequences and Compositions, and LC/MS/MS Analyses—For determination of amino acid sequences of HrUrabins, the LD-DIM fraction was subjected to SDS-PAGE in the presence of thioglycolate, followed by electrophoretic transfer onto a polyvinylidene difluoride membrane. The membrane was cut off and subjected to protein sequence analysis.

For analyses of amino acid compositions, the 35- and 50-kDa HrUrabin bands in LD-DIM fraction, which were separated by SDS-PAGE, were excised, extracted, and subjected to acid hydrolysis (6 N HCl in *in vacuo*, 24 h). The hydrolysate, thus prepared, was subjected to amino acid analysis using a JEOL JLC/500V amino acid analyzer.

The 35- and 50-kDa protein bands were subjected to reduced carboxymethylation with monoiodoacetic acid, and then digested with trypsin (Trypsin Gold, Mass Spectrometry Grade, Promega) according to a procedure described previously (20). Trypsin-digested fragments were subjected to high performance liquid chromatography with a C18 reverse phase column at a constant flow rate of 200 nl/min. After applying the sample to the column (0.05 × 150 mm), which had been equilibrated with 0.1% formic acid containing 2% acetonitrile, the column was washed with equilibration buffer and eluted by a linear gradient of acetonitrile from 2 to 50% in 60 min. The eluate was automatically subjected to an ESI-MS/MS with an LTQ (Thermo, Fisher Scientific).

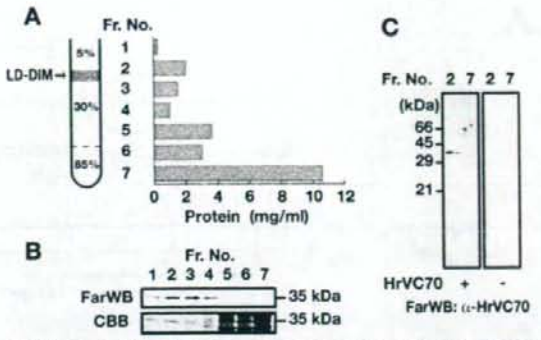

FIGURE 1. **Detection of a sperm membrane-associated binding partner for HrVC70.** *A*, preparation of sperm LD-DIM fraction. The LD-DIM fraction was obtained in a boundary between the 5 and 30% sucrose layers. *B*, each fraction was subjected to SDS-PAGE and Coomassie Brilliant Blue (*CBB*) staining (*lower panel*). The gel was blotted onto a nitrocellulose membrane and subjected to Far Western blotting (*FarWB*), in which the membrane was incubated with HrVC70 and the HrVC70-interacting proteins were detected by anti-HrVC70 antibody and ECL detection kit (*upper panel*). *C*, fractions *2* (LD-DIM fraction) and *7* were blotted onto a nitrocellulose membrane and subjected to the above Far Western analysis in the presence (*left blot*) or absence (*right blot*) of incubation with HrVC70.

Fertilization and Beads Binding Experiments—To avoid any nonspecific inhibitory effect on fertilization caused by serum ingredients, purified anti-HrUrabin polyclonal antibody was used for the following experiments. Antibody purification was carried out using Protein A-Sepharose beads (Sigma).

For the fertilization experiments, sperm were preincubated with anti-HrUrabin antibody or non-immune control antibody for 30 min at 13 °C. Into the sperm suspension (100 μl), a small volume of egg suspension was added and incubated at 13 °C. Fertilization ratio was determined by examining the expansion of perivitelline space, 30–60 min after insemination.

For bead-binding experiments, isolated HrVC70 from the VC was conjugated to the Protein A-Sepharose beads via the anti-HrVC70 antibody as described previously (13). Self- or nonself-sperm suspensions in artificial seawater, which had been incubated for 30 min at 13 °C with control or anti-HrUrabin antibodies at a concentration of 2 mg/ml, was added into a small volume of HrVC70 beads. After the incubation and gentle washes with seawater, sperm were cross-linked onto the beads with 2% paraformaldehyde, and stained with 4′,6-diamino-2-phenylindole. The number of sperm bound to a single agarose bead (50–100 beads were examined for each batch) was counted under a light or fluorescent microscope.

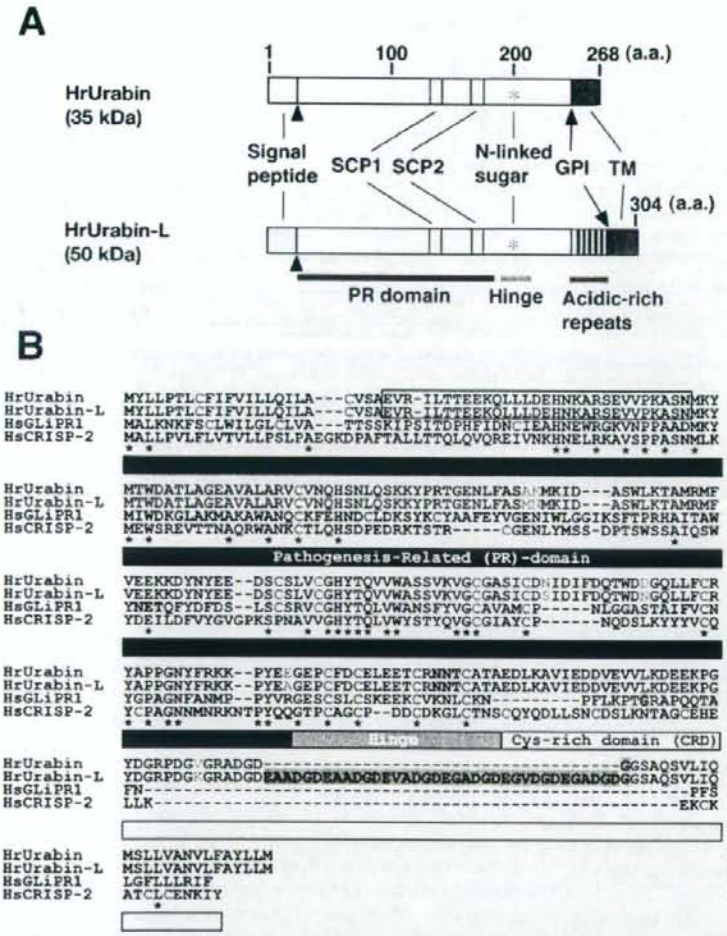

FIGURE 2. **Deduced amino acid sequences of HrUrabin and HrUrabin-L.** *A*, schematic representation of HrUrabin proteins. *Light gray box*, signal peptide; *arrowhead*, predicted cleaved site of the signal peptide; *yellow box*, SCP motif; *blue asterisks*, potential *N*-linked glycosylation site; *gradated gray boxes*, acidic-rich repeat; *dark gray box*, a cleavable transmembrane domain. Abbreviations: *GPI*, glycosylphosphatidylinositol-anchor attachment site; *PR*, PR (plant pathogenesis related-1) domain conserved in CRISPs; *SCP*, sperm coating glycoprotein motif, which is comprised with two separate (SCP1 and 2) sequence signatures; *TM*, transmembrane domain. *B*, a sequence alignment of HrUrabin and HrUrabin-L with human GLIPR1 and CRISP-2. An *open box* in the alignment, initially determined N-terminal sequence of the 35-kDa HrUrabin; *yellow highlight*, SCP motif; *blue highlight*, potential *N*-linked glycosylation site; *red highlight*, acidic-rich repeats; *green highlight*, GPI-anchor attachment site. Note that HrUrabin, HrUrabin-L, and HsGLIPR1 lack C-terminal CRD. Non-conserved residues between HrUrabin and HrUrabin-L, which can be used to distinguish respective peptide fragments by mass spectrometric analysis, are indicted by *blue letters*, whereas Cys residues are indicated by *red letters*. *Asterisks* indicate identical amino acids among these proteins.

RESULTS

Identification of a Binding Partner (HrUrabin) for HrVC70—In sea urchin sperm, most surface proteins that are involved in gamete interaction are known to reside on a LD-DIM fraction or lipid raft fraction (18, 19). According to the protocol for sea urchin sperm (18, 19), we prepared the LD-DIM fraction from *H. roretzi* sperm (Fig. 1*A*). These fractions were subjected to SDS-PAGE and transferred to a nitrocellulose membrane, followed by incubation with HrVC70. HrVC70-interacting proteins on the membrane were detected by an anti-HrVC70 antibody. This Far Western analysis revealed that HrVC70 specifically recognizes a 35-kDa protein from the LD-DIM fraction (Fig. 1, *B* and *C*, *fraction 2*) but not other membrane proteins mainly fractionated in fraction 7. The interaction between these proteins appeared to be enhanced in artificial seawater or high-ionic strength buffer (3× PBS) rather than in 1× PBS (data not shown), suggesting that the interaction is achieved under physiological seawater conditions.

To identify this protein, the 35-kDa protein on a polyvinylidene difluoride membrane was cut out and subjected to protein sequence analysis. On the basis of the determined N-terminal 30 residues (EVRILTTEEKQLLLDEHNKARSEVVPKAXN), two degenerate primers were synthesized, and 3′-RACE and 5′-RACE were carried out. A cDNA library was screened with the obtained RACE clone, yielding two similar but not identical cDNA clones, which encoded the same sequence to the N-terminal sequence of the 35-kDa protein. We designated these genes *HrUrabin* (*Halocynthia roretzi* unique raft-derived binding protein for HrVC70) and *HrUrabin-L* (a long isoform). Schematic representations (*A*) and deduced amino acid sequences (*B*) of HrUrabin and HrUrabin-L are depicted in Fig. 2. These *HrUrabin* and *HrUrabin-L* are novel genes, showing a similarity to *HrTT-1* (21), which was characterized as a gene exclusively expressed in the tail tip of tailbud embryos of *H. roretzi*. Both HrUrabin and HrUrabin-L contain a signal peptide, a PR (plant pathogenesis-related 1) domain, which is well conserved in the CRISP (Cys-rich secretory protein) family with two sperm-coating glycoprotein (SCP) motifs, and a single *N*-glycosylation site, (and six acidic-rich repeats at the C-terminal side only in HrUrabin-L), which is followed by a GPI-anchor attachment site and a cleavable transmembrane domain (Fig. 2). Unlike HrVC70, both HrUrabin and HrUrabin-L were not so polymorphic among different individuals (data not shown). The molecular masses of unmodified HrUrabin and HrUrabin-L were esti-

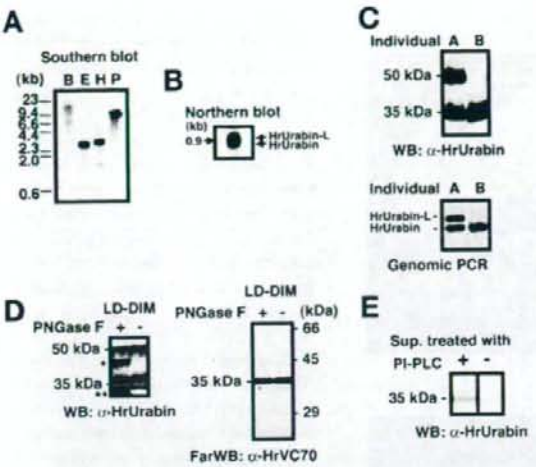

FIGURE 3. **Genomic Southern, Northern, Western, and Far Western blottings of HrUrabin and HrUrabin-L, both of which are GPI-anchored proteins having an *N*-linked sugar.** *A*, Southern blotting of *HrUrabin* on genomic DNAs digested with BamHI (*B*), EcoRI (*E*), HindIII (*H*), and PstI (*P*) restriction enzymes. *B*, Northern blotting of *HrUrabin* in *H. roretzi* gonad. The two bands of *HrUrabin* and *HrUrabin-L* were not differentiated under these experimental conditions. *C*, Western blotting (*WB*) and genomic PCR analysis of HrUrabins on two individuals. The *B* individual showed neither a 50-kDa band in the Western blot nor an HrUrabin-L band in the genomic PCR, suggesting that *HrUrabin-L* encodes the 50-kDa protein and that it does not play an essential role in fertilization. *D*, Western (*left*) and Far Western (*right*) blots of the sperm LD-DIM fraction treated with PNGase-F. The PNGase-F treatment decreases the molecular sizes of both HrUrabins (*left*), but only intact HrUrabin, retaining an *N*-linked carbohydrate, shows a binding ability to HrVC70. *E*, supernatant of the PI-PLC-treated sperm was subjected to Western blotting using anti-HrUrabin antibody. Note that HrUrabin and HrUrabin-L (data not shown) are GPI-anchored proteins, which are exposed, at least in part, on the sperm surface.

mated to be 30,008 and 33,362 Da, respectively. On the other hand, the molecular masses of the mature forms, lacking a signal peptide and a C-terminal portion of GPI-anchor attachment site, and containing a GPI-anchor (~2 kDa), were estimated to be 27 and 30 kDa, respectively.

Expression and Localization of HrUrabins—Southern blotting probed with an *HrUrabin* cDNA, which reacts with both isoforms, using the genomic DNAs digested with several restriction enzymes gave a single band in each lane (Fig. 3*A*), suggesting that the copy number of these genes seems to be single or very low. To determine whether these genes are independent, we isolated several genomic clones containing the *HrUrabin*-derived sequence by screening a λ phage genomic library. We found that several clones contained both genes (data not shown). This indicates that *HrUrabin* and *HrUrabin-L* are two distinct gene copies rather than splice variants of a single gene, being located adjacently within ~20-kbp in the genome of *H. roretzi*.

Northern blotting showed that about 0.9-kb *HrUrabin* mRNAs are expressed in gonad, although two mRNA species were scarcely separated under these conditions (Fig. 3*B*). The results of whole mount *in situ* hybridization also revealed that *HrUrabin* mRNAs are specifically expressed in the testis but not in the ovary (compare Fig. 4, *A* and *B*). Immunocytochemistry using a specific antibody, raised in a rabbit against glutathione *S*-transferase fusion protein, revealed the patch-like localization of HrUrabin on the surface of the sperm head and tail (Fig. 4, *C* and *D*).

HrUrabin and HrUrabin-L Genes Encode the 35- and 50-kDa Proteins, Respectively—Anti-HrUrabin antibody reacted not only to the original 35-kDa protein but also to a novel 50-kDa protein by Western blotting (Fig. 3*C*, *upper panel*, *left lane*). To identify this novel protein, we first determined the N-terminal sequence. The main sequence of its N-terminal five residues was identical to that of 35-kDa HrUrabin, suggesting that the 50-kDa protein is not a cross-reacted unrelated protein but an isoform of HrUrabin. We next analyzed the amino acid compositions of both isoforms. The amino acid composition of the 50-kDa protein did not coincide with the number of amino acids deduced from a cDNA of *HrUrabin-L* or *HrUrabin*, although the amino acid composition of the 35-kDa protein coincided well with the number of amino acids deduced from a cDNA of *HrUrabin* sequence (data not shown).

To examine whether or not the 50-kDa protein is encoded by *HrUrabin-L*, trypsin-digested fragments of the reduced and carboxymethylated 50- and also 35-kDa proteins were separated by reversed phase high performance liquid chromatography, followed by electrospray ionization mass spectrometry (ESI-MS). Each peptide was identified by subsequent tandem mass spectrometry (MS/MS). The results clearly showed that the 50-kDa protein is a gene product of *HrUrabin-L* (Fig. S1) and also confirmed that the 35-kDa protein is a gene product of *HrUrabin*. HrUrabin and HrUrabin-L showed amino acid substitutions at 6 positions (*blue letters* shown in Fig. 2*B*), among which only Val^{237} and Lys^{237} were found to be characteristic to HrUrabin and HrUrabin-L, respectively, because a Val^{237}-containing peptide (number 24′) and a Lys^{237}-containing peptide (numbers L23′) occur only in the 35- and 50-kDa proteins, respectively (see Fig. S1). Another 5 substitutions were polymorphisms commonly observed in HrUrabin and HrUrabin-L, which was revealed by LC/MS/MS analysis.

During the course of this study, we noticed that a few individuals (at a ratio of ~5–10%) expressed neither the 50-kDa protein detected by Western blotting nor the *HrUrabin-L* gene copy detected by genomic PCR analysis (see Fig. 3*C*, *right lanes*). These results agreed with our previous conclusion that the 50-kDa protein is encoded by *HrUrabin-L*. In addition, this also indicates that HrUrabin-L is not essential for fertilization in *H. roretzi*.

Posttranslational Modifications of HrUrabin and HrUrabin-L—Because the molecular sizes of HrUrabin and HrUrabin-L, which were estimated by SDS-PAGE, were higher than those deduced from their cDNA sequences, it is likely that these proteins are posttranslationally modified. This is partly due to the existence of an *N*-linked carbohydrate moiety occurring in both HrUrabin and HrUrabin-L (Fig. 2), because ~3–5-kDa lower molecular mass bands were observed in both proteins under SDS-PAGE after the treatment with PNGase F (Fig. 3*D*, *left*). This *N*-linked sugar chain is essential for the binding of HrUrabin to HrVC70, because deglycosylated 35-kDa HrUrabin failed to bind to HrVC70 in Far Western analysis (compare *left* and *right panels* in Fig. 3*D*). Neither intact nor deglycosylated 50-kDa HrUrabin-L was capable of binding to HrVC70 (Fig. 3*D*).

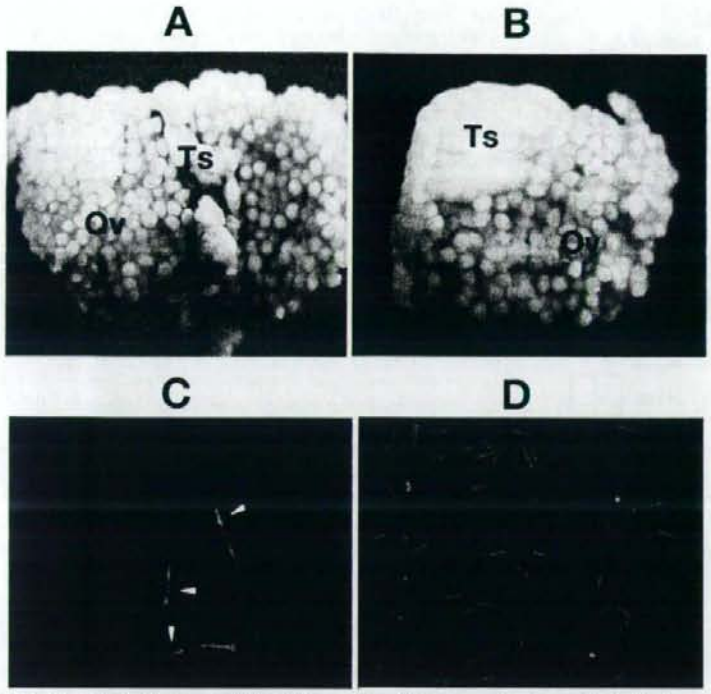

FIGURE 4. ***In situ* hybridization of HrUrabin in gonad and immunocytochemistry of HrUrabin in sperm.** *A* and *B*, a gonad specimen containing testis and ovary was hybridized with antisense (*A*) and sense (*B*) probes for *HrUrabin* mRNA. *HrUrabin* mRNA is expressed in testis but not in ovary. *C* and *D*, immunocytochemistry of *H. roretzi* sperm with anti-HrUrabin (*C*) and control (*D*) antibodies. HrUrabin proteins showed patch-like localization on the surface throughout the sperm as revealed by Alexa Fluor 568-conjugated goat anti-rabbit IgG antibody used as a secondary antibody. Nucleus was stained with 4′,6-diamino-2-phenylindole. *Arrowhead*, sperm head region.

Because both isoforms of HrUrabin contained a GPI-anchor attachment site, we examined the susceptibility of these proteins on the sperm surface to PI-PLC. We found that HrUrabin and HrUrabin-L were partially released from the intact sperm surface by treatment with PI-PLC, which was detected by Western blotting (Fig. 3*E* for HrUrabin, data not shown for HrUrabin-L). We thus conclude that HrUrabin and HrUrabin-L are GPI-anchored proteins, which are exposed on the sperm cell surface.

Roles of HrUrabin in Fertilization and Allorecognition—To investigate the roles of HrUrabin in fertilization, we examined the effects on fertilization of an anti-HrUrabin antibody. As shown in Fig. 5*A*, anti-HrUrabin antibody but not the control antibody specifically inhibited fertilization in a concentration-dependent manner. The inhibitory effect on fertilization was also observed by anti-HrVC70 antibody (data not shown). In addition, we found that anti-HrUrabin antibody potently inhibited the molecular interaction between HrUrabin and HrVC70 on a nitrocellulose membrane (Fig. 5*B*). These results indicate that the apparent association of HrVC70 to a 35-kDa protein(s) on a membrane is certainly due to the interaction between HrVC70 and HrUrabin and that the inhibitory effect of anti-HrUrabin antibody on fertilization is caused by blocking the interaction between HrUrabin and HrVC70.

We previously reported that sperm of *H. roretzi* were able to bind to HrVC70 that is immobilized to protein A-agarose with the aid of anti-HrVC70 antibody (13). The number of nonself-sperm bound to these beads was significantly higher than that of self-sperm bound to the same beads (13). We repeated this experiment using a newly produced anti-HrVC70 antibody, and confirmed that an allorecognizable sperm binding to HrVC70 was reproducibly observed (Fig. 5*C*, comparison between *lanes 1* and *4*). Although the number of sperm bound to HrVC70-agarose was variable among individuals (or batches) (data not shown), the binding of nonself-sperm was significantly higher than that of self-sperm in most cases. The binding of self-sperm to HrVC70, which is immobilized to anti-HrVC70-adsorbed Protein A-agarose (*lane 1*), was observed, but not in the case of unmodified agarose (*lane 7*) or anti-HrVC70-adsorbed Protein A-agarose without immobilizing HrVC70 (*lane 8*). These results coincided with our previous observation that self-sperm also adhere to the VC of intact eggs under physiological conditions (9–11).[1] Anti-HrUrabin antibody potently inhibited the higher affinity of nonself-sperm to HrVC70 (Fig. 5C, comparison between *lanes 4* and *6*), whereas control antibody showed no significant inhibition (comparison between *lanes 4* and *5*). The binding of self-sperm to HrVC70 was also strongly inhibited by anti-HrUrabin antibody (Fig. 5C, *lane 3*) but not by control antibody (*lane 2*).

As mentioned earlier, HrUrabin and HrUrabin-L are not highly polymorphic. Therefore, we examined whether the binding of HrVC70 to HrUrabin on a nitrocellulose membrane is allospecific or not, by using HrVC70 and sperm LD-DIM fractions, both of which were prepared from the same and different individuals. As shown in Fig. 5*D*, no significant differences were observed between autologous and allogeneic interactions between HrUrabin and HrVC70 in several combinations. These results suggest that HrUrabin is not a direct allorecognition molecule, although this protein seems to be indispensable for self-incompatible fertilization in *H. roretzi*.

DISCUSSION

Difference in the Results by Far Western Analysis and Yeast Two-hybrid Screening—The present paper demonstrated that a sperm 35-kDa GPI-anchored CRISP-like glycoprotein, referred

[1] H. Sawada, unpublished observation.

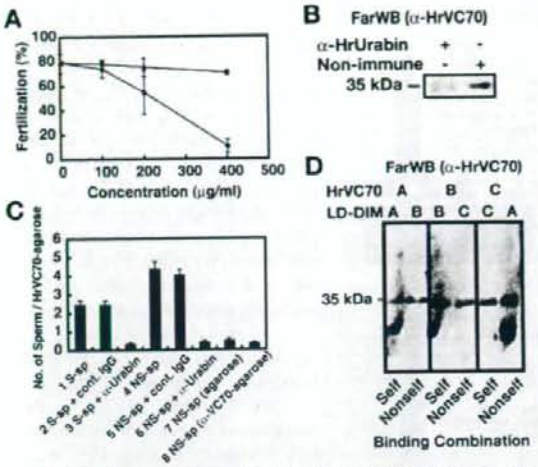

FIGURE 5. **Involvement of sperm HrUrabin in fertilization and allorecognizable sperm binding to HrVC70.** *A*, the concentration-dependent inhibitory effect of anti-HrUrabin antibody on fertilization. A small volume of egg suspension was added into a sperm suspension, which had been preincubated with anti-HrUrabin antibody (*closed circle*) or control antibody (*closed square*). Fertilization ratio was determined on the basis of the expansion of perivitelline space. *Error bars* indicate the standard deviation ($n = 3$). *B*, inhibitory effect of anti-HrUrabin antibody on the binding of HrVC70 to HrUrabin on a membrane. Biotin-labeled anti-HrVC70 antibody was used for the detection. *C*, inhibitory effect of anti-HrUrabin antibody on the binding of sperm to HrVC70-coated agarose beads. Self-sperm (*S-sp*) or nonself-sperm (*NS-sp*) suspension, which had been incubated with control (*cont. IgG*) or anti-HrUrabin (*α-Urabin*) antibodies, was added into a small volume of suspension of HrVC70-coated agarose beads (no mark), Protein A-beads alone (*agarose*), or anti-HrVC70-conjugated beads without HrVC70 (*α-VC70-agarose*). The number of sperm bound to a single agarose bead was counted for 50–100 beads. In the control experiments (*lanes 7* and *8*), no significant sperm binding above the background level was detected. *Error bars* indicate the standard error ($n = 50$). *D*, interaction between HrVC70 and HrUrabin is not allo-specific. Sperm LD-DIM fractions prepared from individuals A, B, and C, were subjected to Far Western analyses using HrVC70 suspensions prepared from the same individuals.

to as HrUrabin, in the LD-DIM fraction is a binding partner for HrVC70 on the VC of the eggs in *H. roretzi*. Our previous yeast two-hybrid screening failed to identify HrUrabin (16). A possible reason for this is that a carbohydrate moiety, which is essential for the binding between HrVC70 and HrUrabin (Fig. 3*D*), may not be properly attached to HrUrabin in yeast cells. On the other hand, HrTTSP-1, which was identified as an HrVC70-interacting protein by yeast two-hybrid screening (16), was not detected by Far Western analysis. Ionic detergent (0.1% SDS), which was used for solubilization of HrVC70, might impair the interaction between HrUrabin and HrTTSP-1 in Far Western analysis. Our present results do not rule out the possibility that HrTTSP-1 is involved in fertilization. Actually, a certain processing product of HrTTSP-1 was found to occur in sperm exudates (a supernatant of activated sperm by alkaline seawater), implying its participation in fertilization.[5] Therefore, it seems to be plausible that both HrUrabin and HrTTSP-1 are involved in gamete interaction. But, taking into account the inhibitory effects of anti-HrUrabin antibody on fertilization and allorecognizable sperm binding to HrVC70-agarose, it should be emphasized that at least HrUrabin plays a key role in allorecognizable sperm binding to the VC during fertilization.

Functions of HrUrabin and Other CRISP Members in Fertilization—Physiological functions of CRISP family proteins are poorly understood. One of the most characterized CRISPs is an epididymal glycoprotein CRISP-1 (DE), which is associated with the sperm surface and is predicted to play a role in gamete fusion (22). The PR domain is reported to be a binding region of CRISP-1 to the egg surface (23). On the other hand, it is also reported that the PR domain functions as a protease in a specific CRISP member (24). In contrast, our results suggest that HrUrabin plays a pivotal role in the primary binding of sperm to HrVC70, a sperm receptor on the VC, rather than gamete fusion, during fertilization. In macaque, it is reported that an antibody raised against sperm surface protein, which is released by treatment with PI-PLC, revealed the existence of GPI-anchored CRISP on the sperm membrane, possibly participating in fertilization (25). This protein exists in two isoforms with molecular masses of 24 and 48 kDa, similarly to HrUrabin, although they assumed that the 48-kDa isoform is a dimer of the 24-kDa isoform (25). As mentioned above, CRISP members on the sperm surface seem to play diverse roles in fertilization in different species.

HrVC70 consists solely of 12 tandem EGF-like repeats. Although the EGF motif is widely distributed in many extracellular proteins involved in intermolecular interactions, little is known about their physiological binding partners. Our present finding revealed for the first time that a CRISP-like glycoprotein is a novel ligand for EGF modules. The ascidian *C. intestinalis* also has multiple genes encoding both EGF and zona pellucida domains (26), but such proteins are not known as egg-coat proteins in animals other than ascidians. Whether the interaction between CRISP-like glycoprotein and the EGF module is involved in fertilization of *C. intestinalis*, and also in other protein-protein interactions is an intriguing issue remaining to be studied.

Possible Posttranslational Modification in HrUrabin-L—Because the amino acid composition of the 50-kDa protein (50-kDa HrUrabin-L) did not coincide with the number of amino acids deduced from *HrUrabin-L* cDNA (data not shown), and also because the trypsin-digested fragments of 50-kDa HrUrabin-L showed no peptide-12/L20 by LC/MS/MS analysis (see Fig. S1), yet unknown posttranslational modification may occur in the 50-kDa protein in addition to the N-glycosylation and the attachment of GPI-anchor. In connection with this, it is interesting to note our preliminary observation that a non-catalytic domain, a L1 (ΔL2) region (Ser^{23}–Asn^{96}) of the light chain (L-chain), of a sperm trypsin-like protease HrSpermosin, which is involved in sperm binding to and penetration through the VC during fertilization (27), seems to be tightly or covalently bound to 50-kDa HrUrabin-L. Anti-L1 (ΔL2) antibody, but not anti-L2 (Ser^{97}–Lys^{129}) antibody, reacted to 50-kDa HrUrabin-L, whereas anti-L1(ΔL2) antibody showed no reactivity to the bacterially expressed glutathione *S*-transferase-HrUrabin-L fusion protein. Furthermore, the 50-kDa band on a membrane was not detected by Western blotting using anti-L1(ΔL2) antibody in the cases of

[5] H. Hyodo, N. Yokota, and H. Sawada, unpublished data.

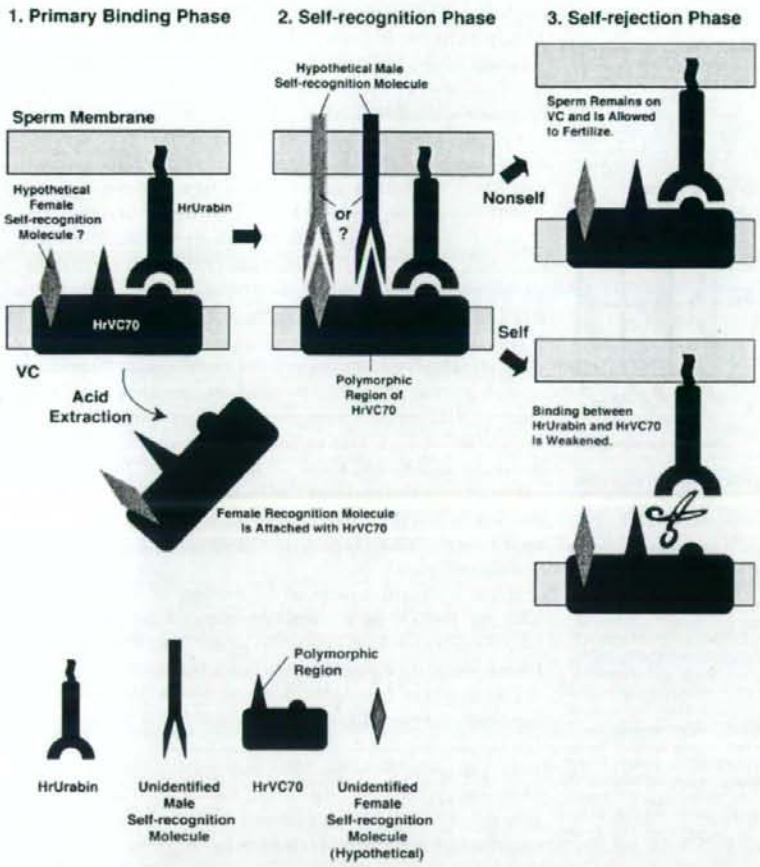

FIGURE 6. **A working hypothesis on the role of HrUrabin in gamete interaction.** *1*, primary binding phase: HrUrabin on the sperm lipid rafts binds to HrVC70 on the VC, probably via the non-polymorphic region of HrVC70 (13). *2*, self-recognition phase: unidentified sperm-borne self-recognition molecule recognizes polymorphisms of HrVC70 or an unknown hypothetical polymorphic binding partner tightly associated with HrVC70. If the latter possibility is the case, HrVC70-conjugated beads used in the bead-binding experiments may also contain such a female self-recognition molecule. *3*, self-rejection phase: if the self-recognition between male and female recognition molecules does not occur, and also if the sperm recognizes HrVC70 (or its complex) as nonself, the sperm-borne lysin system may be activated, allowing the sperm passage through the VC. On the other hand, if the sperm recognizes the HrVC70 (or its complex) as self, a downstream signaling pathway is activated, resulting in the detachment of sperm from the VC. It seems likely that some unidentified proteases or glycosidases are involved in this weakening process: HrVC70 or/and HrUrabin may be a target of such hydrolytic cleavages because their interaction is considered to be a main force of the primary gamete interaction. Although no appreciable difference in the sperm binding to the VC has been observed between autologous and allogeneic gamete combinations, it is plausible that sperm detached from self-HrVC70 may continue to loosely adhere to the VC, due to the adhesive nature of the VC in this species and also a possible interaction between sperm and the VC, which is mediated by sperm fucosidase (30).

HrUrabin-L-missing individuals.[6] These results suggest that 50-kDa HrUrabin-L is a molecular species covalently linked with L1(ΔL2) peptide of HrSpermosin. Because the VC-lysin system responsible for sperm penetration of the VC must be activated after sperm recognizes the VC as nonself, covalent linkage between HrUrabin and HrSpermosin may be coupled to accomplish "the allorecognition-linked lysin system" during ascidian fertilization.

[6] M. Akasaka, Y. Harada, and H. Sawada, unpublished data.

Self/Nonself Recognition Mechanisms during Ascidian Fertilization—Molecular mechanisms of self-incompatibility in higher plants have been studied well in various species. In Brassicaceae, it is controlled by *S*-locus, which has multiple alleles, and each allele encodes male and female recognition molecules, which enables an allele-specific interaction (28). The self/nonself discrimination between the male and female recognition molecules takes place on the basis of recognition (and then rejection) of "self" in these species (1, 28). We recently revealed the molecular mechanism of the self-incompatibility system in the ascidian *C. intestinalis* (29). In *C. intestinalis*, two unlinked loci are involved in its self-sterility, both of which encode a pair of polycystin-1-like receptors on the sperm surface (s-Themis-A and -B) and fibrinogen-like ligand on the VC (v-Themis-A and -B). Our genetic analysis revealed that the system in *C. intestinalis* is based on the recognition of self-ligands (v-Themis) by their respective receptors (s-Themis). Because the VC of *C. intestinalis* eggs exhibits higher affinity to nonself-sperm than to self-sperm, self-sperm must be detached from the VC when the recognition molecule on the sperm surface finds the self-ligand on the VC. This self-incompatibility system is very similar to those of higher plants, in which pollen tube elongation is blocked when it is recognized as self in the stigma.

Here, we propose a working hypothesis on the self-sterility in *H. roretzi* (Fig. 6). In this hypothesis, the self-incompatible fertilization process consists of three phases. In the first phase (primary binding phase), both self- and nonself-sperm equally bind to the VC. Because anti-HrUrabin antibody abolished the basal binding of self-sperm to HrVC70 beads, the interaction between HrUrabin and HrVC70 seems to be essential for the primary gamete interaction. After this phase, a self-recognition process between a male-recognition molecule on the sperm surface and a female-recognition molecule on the VC may take place (self-recognition phase). When the male side molecule recognizes the self-ligand on the VC, the primary binding ability of sperm must be decreased (self-rejection phase). The interaction

between HrVC70 and sperm-surface HrUrabin must be weakened in autologous gamete combination, but the molecular interaction between HrUrabin and HrVC70 would not change on the basis of Far Western analysis. This must be an important factor why HrUrabin shows equivalent affinity for self- and nonself-derived HrVC70 by Far Western analyses. HrUrabin may play a key role in several processes during self-incompatible fertilization, although HrUrabin itself is unlikely to be a direct allorecognition molecule. It is thought that HrUrabin is involved in the primary binding phase, which is essential for the onset of the self-recognition process. It appears to have a crucial role also in the self-rejection phase, because the affinity of sperm surface HrUrabin to HrVC70 must be lowered after the sperm recognizes the self-ligand (HrVC70 or its complex) on the VC. Difference in sperm binding ability to the VC between autologous and allogeneic gamete combinations, which is well known in *C. intestinalis* (7), is not obvious in *H. roretzi* (10). Presumably, sperm may loosely adhere to the VC even after the detachment from self-HrVC70, due to the adhesive nature of the VC in this species. In addition, a sperm α-L-fucosidase-mediated interaction between sperm and the VC (30) may also contribute to this autologous adhesion.

We assume that a putative sperm-borne self-recognition molecule must specifically recognize the autologous HrVC70. However, such a self-recognition protein has not yet been identified in *H. roretzi*. Although the polymorphisms of HrVC70 may provide a molecular basis of allorecognition, another possibility is also considered: a hypothetical molecule tightly associated with HrVC70 may be involved in self-recognition (see Fig. 6). Such a putative molecule might be co-extracted with weak acid and immobilized to agarose beads. Whether homologs of *C. intestinalis* self-incompatibility genes (two pairs of s-/v-Themis) encode sperm- and VC-derived self-recognition molecules in *H. roretzi*, and also whether homologs of HrUrabin and HrVC70 are involved in the self-incompatible fertilization in *C. intestinalis* are very intriguing issues remaining to be solved.

Acknowledgments—We are grateful to the director and the staffs of the Research Center for Marine Biology, Graduate School of Life Sciences, Tohoku University, where part of this work was carried out. We are indebted to T. Hirose of the Center for Instrumental Analysis, Hokkaido University, where protein sequence and amino acid composition analyses were carried out. We are grateful to Charles and Gretchen Lambert for helpful comments and critical reading of this manuscript.

REFERENCES

1. Harada, H., and Sawada, H. (2008) *Int. J. Dev. Biol.* **52,** in press
2. Jiang, D., and Smith, W. C. (2005) *Biol. Bull.* **209,** 107–112
3. Morgan, T. H. (1923) *Proc. Natl. Acad. Sci. U. S. A.* **9,** 170–171
4. Morgan, T. H. (1939) *J. Exp. Zool.* **80,** 19–54
5. Morgan, T. H. (1942) *J. Exp. Zool.* **90,** 199–228
6. Morgan, T. H. (1944) *J. Exp. Zool.* **95,** 37–59
7. Rosati, F., and De Santis, R. (1978) *Exp. Cell Res.* **112,** 111–119
8. Sawada, H. (2002) *Zool. Sci.* **19,** 139–151
9. Fuke, T. M. (1983) *Roux's Arch. Dev. Biol.* **192,** 347–352
10. Fuke, M., and Numakunai, T. (1996) *Roux's Arch. Dev. Biol.* **205,** 391–400
11. Fuke, M., and Numakunai, T. (1999) *Mol. Reprod. Dev.* **52,** 99–106
12. Sawada, H., Sakai, N., Abe, Y., Tanaka, E., Takahashi, Y., Fujino, J. Kodama, E., Takizawa, S., and Yokosawa, H. (2002) *Proc. Natl. Acad. Sci. U. S. A.* **99,** 1223–1228
13. Sawada, H., Tanaka, E., Ban, S., Yamasaki, C., Fujino, J., Ooura, K., Abe, Y., Matsumoto, K., and Yokosawa, H. (2004) *Proc. Natl. Acad. Sci. U. S. A.* **101,** 15615–15620
14. Artavanis-Tsakonas, S., Matsuno, K., and Fortini, M. E. (1995) *Science* **268,** 225–232
15. Ioutel, A., Corpechot, C., Ducros, A., Vahedi, K., Chabriat, H., Mouton, P., Domenga, V., Cécillion, M., Marechal, E., Maciazek, J., Vayssiere, C., Cruaud, C., Cabanis, E. A., Ruchoux, M. M., Weissenbach, J., Bach, J. F., Bousser, M. G., and Tournier-Lasserve, E. (1996) *Nature* **383,** 707–710
16. Harada, Y., and Sawada, H. (2007) *Mol. Reprod. Dev.* **74,** 1178–1187
17. Sawada, H., Yokosawa, H., Hoshi, M., and Ishii, S. (1982) *Gamete Res.* **5,** 291–301
18. Ohta, K., Sato, C., Matsuda, T., Toriyama, M., Vacquier, V. D., Lennarz, W. J., and Kitajima, K. (2000) *Glycoconj. J.* **17,** 205–214
19. Ohta, K., Sato, C., Matsuda, T., Toriyama, M., Lennarz, W. J., and Kitajima, K. (1999) *Biochem. Biophys. Res. Commun.* **258,** 616–623
20. Harazono, A., Kawasaki, N., Kawanishi, T., and Hayakawa, T. (2005) *Glycobiology* **15,** 447–462
21. Hotta, K., Takahashi, H., and Satoh, N. (1998) *Dev. Genes Evol.* **208,** 164–167
22. Ellerman, D. A., Cohen, D. J., Da Ros, V. G., Morgenfeld, M. M., Busso, D., and Cuasnicú, P. S. (2006) *Dev. Biol.* **297,** 228–237
23. Roberts, K., Ensrud, K. M., Wootres, J. L., Nolan, M. A., Johnston, D. S., and Hamilton, D. W. (2006) *Mol. Cell. Endocrinol.* **250,** 122–127
24. Milne, T. J., Abbenante, G., Tyndall, J. D., Halliday, J., and Lewis, R. J. (2003) *J. Biol. Chem.* **278,** 31105–31110
25. Yudin, A. I., Li, M.-W., Robertson, K. R., Tollner, T., Cherr, G. N., and Overstreet, J. W. (2002) *Mol. Reprod. Dev.* **63,** 488–499
26. Kurn, U., Sommer, F., Bosch, T. C., and Khalturin, K. (2007) *Dev. Comp. Immunol.* **31,** 1242–1254
27. Kodama, E., Baba, T., Kohno, N., Satoh, S., Yokosawa, H., and Sawada, H. (2002) *Eur. J. Biochem.* **269,** 657–663
28. Takayama, S., and Isogai, A. (2005) *Annu. Rev. Plant Biol.* **56,** 467–489
29. Harada, Y., Takagaki, Y., Sunagawa, M., Saito, T., Yamada, L., Taniguchi, H., Shoguchi, E., and Sawada, H. (2008) *Science* **320,** 548–550
30. Matsumoto, M., Hirata, J., Hirohashi, N., and Hoshi, M. (2002) *Zool. Sci.* **19,** 43–48

THE JOURNAL OF BIOLOGICAL CHEMISTRY VOL. 283, NO. 48, pp. 33036–33045, November 28, 2008
© 2008 by The American Society for Biochemistry and Molecular Biology, Inc. Printed in the U.S.A.

N-Glycosylation of Laminin-332 Regulates Its Biological Functions

*A NOVEL FUNCTION OF THE BISECTING GlcNAc**

Received for publication, June 13, 2008, and in revised form, September 11, 2008 Published, JBC Papers in Press, September 23, 2008, DOI 10.1074/jbc.M804526200

Yoshinobu Kariya[‡], Rika Kato[‡], Satsuki Itoh[§], Tomohiko Fukuda[¶], Yukinao Shibukawa[‖], Noriko Sanzen[‖], Kiyotoshi Sekiguchi[‖], Yoshinao Wada[‖], Nana Kawasaki[§], and Jianguo Gu[‡1]

From the [‡]Division of Regulatory Glycobiology, Institute of Molecular Biomembrane and Glycobiology, Tohoku Pharmaceutical University, 4-4-1 Komatsushima, Aoba-ku, Sendai, Miyagi 981-8558, Japan, [§]National Institute of Health Sciences, 1-81-1, Kamiyoga, Setagaya-ku, Tokyo 158-8501, Japan, [¶]Department of Molecular Medicine, Osaka Medical Center and Research Institute for Maternal and Child Health, 840 Murodo, Izumi, Osaka 594-1101, Japan, and the [‖]Division of Protein Chemistry, Institute for Protein Research, Osaka University, Suita, Osaka 565-0871, Japan

Laminin-332 (Lm332) is a large heterotrimeric glycoprotein that has been identified as a scattering factor, a regulator of cancer invasion as well as a prominent basement membrane component of the skin. Past studies have identified the functional domains of Lm332 and revealed the relationships between its activities and the processing of its subunits. However, there is little information available concerning the effects of *N*-glycosylation on Lm332 activities. In some cancer cells, an increase of β1,6-GlcNAc catalyzed by *N*-acetylglucosaminyltransferase V (GnT-V) is related to the promotion of cancer cell motility. By contrast, bisecting GlcNAc catalyzed by *N*-acetylglucosaminyltransferase III (GnT-III) suppresses the further processing with branching enzymes, such as GnT-V, and the elongation of *N*-glycans. To examine the effects of those *N*-glycosylations to Lm332 on its activities, we purified Lm332s from the conditioned media of GnT-III- and GnT-V-overexpressing MKN45 cells. Lectin blotting and mass spectrometry analyses revealed that *N*-glycans containing the bisecting GlcNAc and β1,6-GlcNAc structures were strongly expressed on Lm332 purified from GnT-III-overexpressing (GnT-III-Lm332) and GnT-V-overexpressing (GnT-V-Lm332) cells, respectively. Interestingly, the cell adhesion activity of GnT-III-Lm332 was apparently decreased compared with those of control Lm332 and GnT-V-Lm332. In addition, the introduction of bisecting GlcNAc to Lm332 resulted in a decrease in its cell scattering and migration activities. The weakened activities were most likely derived from the impaired α3β1 integrin clustering and resultant focal adhesion formation. Taken together, our results clearly demonstrate for the first time that *N*-glycosylation may regulate the biological function of Lm332. This finding could introduce a new therapeutic strategy for cancer.

Laminins (Lms)[2] are large heterotrimeric glycoproteins that are prominent components of basement membranes and are involved in important biological roles, including tissue development and cell differentiation, survival, adhesion, and migration (1). Lms are heavily glycosylated molecules. It has been reported that between 13 and 30% of the total molecular weight of Lms is *N*-linked glycosylated (2). Laminin-111 (Lm111; previously known as laminin-1) is easily purified from mouse Engelbreth-Horm-Swarm tumor and has been intensively investigated for its carbohydrate structures. In comparison with unglycosylated Lm111, which is purified from cell lysates of tunicamycin-treated cells, glycosylation of Lm111 was shown to affect cell spreading and neurite outgrowth activities but not cell adhesion activity or heterotrimer assembly (3, 4). However, tunicamycin extensively inhibited the secretion of laminin into cell culture medium (3, 5).

Laminin-332 (Lm332; previously known as laminin-5) is composed of α3, β3, and γ2 chains. Lm332 is expressed in the skin and other stratified squamous epithelial tissues, where is associate with hemidesmosomes via integrin α6β4. Genetic absence of Lm332 causes a severe and lethal skin blistering disease, Herlitz's junctional epidermolysis bullosa (6, 7). *In vitro* Lm332 promotes cell motility and scattering through the association of C-terminal globular (G) domains with integrin α3β1 (8), which is thought to be a key factor during wound healing (9, 10) and cancer metastasis (11, 12). Proteolytic cleavage of the Lm332 α3 and γ2 subunits (13, 14) affects both cell adhesion and migration (15, 16). Few studies have assessed the functional significance of *N*-glycosylation of Lm332 subunits.

N-Acetylglucosaminyltransferase V (GnT-V) catalyzes the addition of the β1,6-linked GlcNAc branch and defines this subset of *N*-glycans (17, 18) (Fig. 1*A*). In some cancers, an increase of β1,6-GlcNAc is related to cancer metastasis. This is

* This work was supported in part by Core Research for Evolutional Science and Technology (CREST), the Japan Science and Technology Agency (JST), and the Academic Frontier Project for Private Universities from the Ministry of Education, Culture, Sports, Science, and Technology of Japan. The costs of publication of this article were defrayed in part by the payment of page charges. This article must therefore be hereby marked "*advertisement*" in accordance with 18 U.S.C. Section 1734 solely to indicate this fact.

[1] To whom correspondence should be addressed. Tel.: 81-22-727-0216; Fax: 81-22-727-0078; E-mail: jgu@tohoku-pharm.ac.jp.

[2] The abbreviations used are: Lm, laminin; BRL, buffalo rat liver; BSA, bovine serum albumin; CBB, Coomassie Brilliant Blue; ECM, extracellular matrix; E_4-PHA, erythroagglutinating phytohemagglutinin; ELISA, enzyme-linked immunosorbent assay; GnT-III, *N*-acetylglucosaminyltransferase III; GnT-V, *N*-acetylglucosaminyltransferase V; LC, liquid chromatography; L_4-PHA, leukoagglutinating phytohemagglutinin; Lmxyz, laminin-xyz; MS, mass spectrometry; PBS, phosphate-buffered saline; CHAPS, 3-[(3-cholamidopropyl)dimethylammonio]-1-propanesulfonic acid.

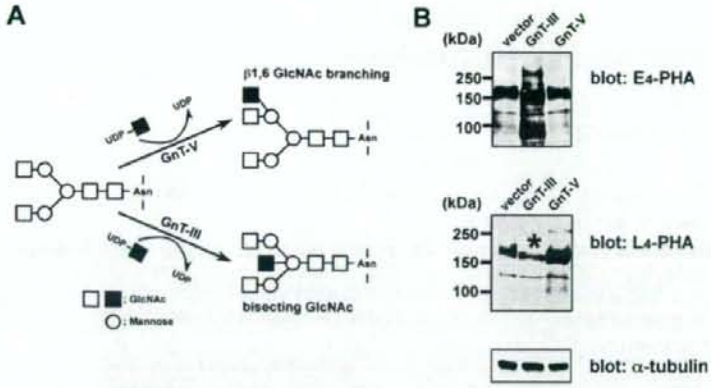

FIGURE 1. **Characterization of MKN45 transfectants overexpressing GnT-III or GnT-V.** *A*, biosynthesis pathways of the bisecting GlcNAc and β1,6-GlcNAc branching structures by GnT-III and GnT-V, respectively. *Square*, *N*-acetylglucosamine; *circle*, mannose. *B*, 20 μg of cell lysates from vector, GnT-III, and GnT-V MKN45 transfectants were run on 7.5% SDS-polyacrylamide gels and then blotted to nitrocellulose membranes. Blotted proteins were probed with biotinylated E_4-PHA lectin (*top*) and L_4-PHA lectin (*middle*). E_4-PHA and L_4-PHA lectin blotting revealed that GnT-III and GnT-V transfectants were significantly modified with bisecting GlcNAc and β1,6-linked GlcNAc, respectively. An *asterisk* indicates reduced L_4-PHA staining in GnT-III transfectants. α-tubulin was used as a loaded control.

supported by several reports, including GnT-V overexpression in cancer (19, 20) and GnT-V-deficient mouse studies (21). By contrast, bisecting GlcNAc catalyzed by *N*-acetylglucosaminyltransferase III (GnT-III) (Fig. 1*A*) suppresses further processing with branching enzymes, such as GnT-V, and elongation of *N*-glycans (22, 23), resulting in down-regulating cancer metastasis (24). In addition, GnT-III modification of α3β1 integrin inhibits cell migration promoted by GnT-V on the Lm332 substrate (25).

In the present study, to investigate the effect of *N*-glycosylation on Lm332 function, we focused on GnT-III- and GnT-V-mediated *N*-glycosylation of Lm332. Therefore, we purified Lm332s from the conditioned media of GnT-III- and GnT-V-overexpressing MKN45 cells. The analysis of lectin blotting and mass spectrometry indicated that Lm332 could be modified by either GnT-III or GnT-V. As a result, GnT-III modification of Lm332 caused a decrease in its keratinocyte cell adhesion and migration activities. Our findings demonstrate a novel regulatory mechanism of Lm332 activities brought on by *N*-glycosylation.

EXPERIMENTAL PROCEDURES

Antibodies and Reagents—Mouse monoclonal antibodies against the N-terminal regions of the human laminin α3 chain (Lsαc3) and the γ2 chain (D4B5) were a generous gift from Dr. Kaoru Miyazaki (Yokohama City University, Yokohama, Japan). Mouse monoclonal antibody against the laminin α3 chain (2B10) was prepared as previously described (26). Monoclonal antibodies against the human laminin β3 chain (kalinin B1) and paxillin were purchased from Transduction Laboratories (Lexington, KY). Control mouse and rat IgG and function-blocking anti-integrin α3 (P1B5) and α6 (GoH3) antibodies were from Santa Cruz Biotechnology, Inc. (Santa Cruz, CA). Alexa Fluor 488 goat anti-mouse IgG was obtained from Invitrogen. Biotinylated leukoagglutinating phytohemagglutinin (L_4-PHA) and biotinylated erythroagglutinating phytohemagglutinin (E_4-PHA) were from Seikagaku Biobusiness Corp. (Tokyo, Japan). A monoclonal antibody against α-tubulin was purchased from Sigma.

Cell Culture—The human gastric cancer cell line MKN45 was cultured in RPMI 1640 medium (Nacalai Tesque, Japan). MKN45 transfectants were described previously (27). The Buffalo rat liver-derived epithelial cell line BRL was a gift from Dr. Kaoru Miyazaki (Yokohama City University, Yokohama, Japan) and was maintained in Dulbecco's modified Eagle's medium. Those media were supplemented with 10% fetal calf serum, penicillin, and streptomycin sulfate. Keratinocytes isolated from patients with junctional epidermolysis bullosa lacking Lm332 were a generous gift from Dr. M. Peter Marinkovich (Stanford University). Keratinocytes were grown in 50% defined keratinocyte medium (Invitrogen) and 50% medium 154 (Cascade Biologics, Portland, OR) containing penicillin and streptomycin sulfate.

Preparation of Conditioned Medium and Purification of Laminin-332—For purification of Lm332, the serum-free CM from MKN45 transfectants were collected every 2 or 3 days. The collected media were centrifuged at 1,000 rpm for 10 min. Finally its supernatant was collected and used as a source for purification of Lm332. The protein containing the supernatant was precipitated by 80% saturated ammonium sulfate. The precipitate was dissolved in and dialyzed against a gelatin column buffer (20 mM Tris-HCl (pH 7.5), 0.1 M NaCl, 0.1% CHAPS, 0.005% Brij 35) overnight at 4 °C. Then samples were centrifuged at 19,000 rpm for 30 min at 4 °C to remove the undissolved proteins. The precleared solution was passed through a gelatin column, and then its flow-through was directly applied to an α3 antibody (2B10) column. After washing with the antibody column buffer (20 mM Tris-HCl (pH 7.5), 0.5 M NaCl, 0.1% CHAPS, 0.005% Brij 35), followed by MilliQ water, binding proteins were eluted by 0.05% trifluoroacetic acid (v/v) and immediately neutralized with Tris-HCl (pH 8.0) containing 0.005% Brij 35 and 0.1% CHAPS.

Preparation of Cell Lysate—For preparing cell lysate, cells were washed with cold PBS twice and then lysed with lysis buffer (1% Triton X-100, 20 mM Tris-HCl (pH 7.4), 150 mM NaCl, 5 mM EDTA) containing protease inhibitor mixture (Nacalai Tesque). After incubation for 10 min on ice, cell lysates were cleared by centrifugation at 15,000 rpm for 10 min at 4 °C, and its supernatants were used in the following samples. The protein concentration was determined using a protein assay kit (Nacalai Tesque).

SDS-PAGE, Immunoblotting, and Lectin Blotting—SDS-PAGE was performed either on 6% gels or on 4.0–7.5% gradient gels under reducing or nonreducing conditions. Separated proteins were stained with Coomassie Brilliant Blue (CBB). Image] software was used for densitometric analysis of protein bands. For immunoblotting analyses, proteins resolved by SDS-PAGE were

transferred to nitrocellulose membranes. The blots were probed with each specific antibody or biotinylated E_4-PHA and L_4-PHA. Immunoreactive bands were detected using an ECL detection kit (GE Healthcare) and a Vectastain ABC kit (Vector Laboratories).

Analysis of N-Glycan Structures by Liquid Chromatography/Multiple-stage Mass Spectrometry (LC/MS^n)—Purified Lm332 was applied to SDS-PAGE using a 4–7.5% gradient gel under reducing conditions and visualized by CBB staining. The gel bands corresponding to α3, β3, and γ2 subunits were excised from the gel and then cut into pieces, respectively. The gel pieces were destained with 25 mM NH_4HCO_3 containing 30% acetonitrile and then dehydrated with 100% acetonitrile. The proteins in the gel were reduced and carboxymethylated by incubation with dithiothreitol and sodium monoiodoacetate (25). *N*-Glycans were released by the treatment with peptide:*N*-glycanase F, and extracted from the gel pieces, as reported (28). The oligosaccharides were reduced with sodium borohydride and desalted. LC/MS^n was performed using a quadropole linear ion trap-Fourier transform ion cyclotron resonance mass spectrometer (Finnigan LTQ-FT™; Thermo Fisher Scientific Corp., San Jose, CA) connected to a nanoflow LC system (NanoFrontier nLC; Hitachi High-Technologies Corp., Japan). The eluents were 5 mM ammonium acetate containing 2% acetonitrile, pH 9.6 (pump A), and 5 mM ammonium acetate containing 80% acetonitrile, pH 9.6 (pump B). The borohydride-reduced *N*-glycans were separated on a Hypercarb column (0.075 × 150 mm; Thermo Fisher Scientific Corp.) with a linear gradient of 5–35% of pump B in 110 min. A single mass scan with Fourier transform (*m/z* 450–2,000) followed by data-dependent MS/MS for the most intense ions was performed in both positive and negative ion modes as previously reported (29).

Cell Adhesion Assay—Cell adhesion assay was performed as described previously (8). Briefly, each well of a 96-well enzyme-linked immunosorbent assay (ELISA) plate (Costar, Cambridge, MA) was coated with a substrate protein and then blocked with 1% bovine serum albumin (BSA). 2×10^4 cells in supplement-free keratinocyte growth medium were inoculated per well of 96-well plates. After nonadherent cells were removed, adherent cells were fixed with 25% (w/v) glutaraldehyde and stained with 0.5% crystal violet (w/v) in 20% (v/v) methanol for 10 min. The well was measured for absorbance at 590 nm using a microplate reader. For inhibition assay, the cell suspension was incubated with function-blocking anti-integrin antibodies or with the control IgG for 20 min at room temperature before inoculation.

Cell Spreading Assay—For measurement of the cell-spreading area, keratinocytes on purified Lm332 substrates were incubated in keratinocyte growth medium. After 1 h, at least 100 cells were photographed, and their cell spreading areas were measured using Axio Vision software (Carl Zeiss, Germany).

Cell Scattering Assay—A scattering assay was done as reported previously (10). Briefly, 500 μl of cell suspension (2×10^4 cells in Dulbecco's modified Eagle's medium plus 1% (v/v) fetal calf serum) were inoculated per well of 24-well plates. Test samples were directly added into the culture medium and incubated at 37 °C. After 40 h, cells were fixed with 25% (w/v) glutaraldehyde and stained with 0.5% crystal violet (w/v) in 20% (v/v) methanol for 10 min. The scattered single cells were counted, and the degree of cell scattering was expressed as the percentage of single cells in each field. At least 300 cells were counted in each field.

Cell Migration Assay—A glass bottom dish (Asahi Techno Glass, Japan) was precoated with purified Lm332 and then blocked with 1% BSA for 1 h at 37 °C. 200 μl of Lm332-null keratinocyte cell suspension (4×10^4 cells/ml) in growth medium were inoculated into each Lm332-precoated glass bottom dish. After incuba-

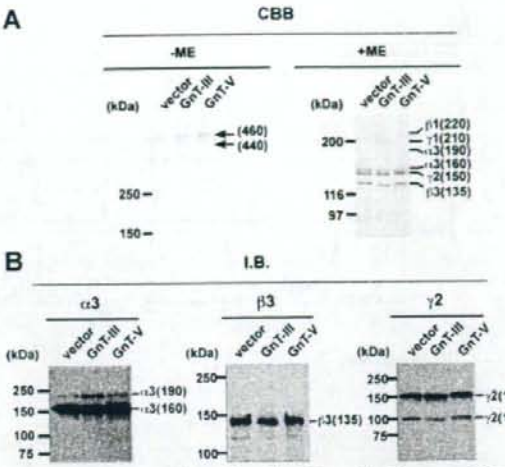

FIGURE 2. **Characterization of laminin-332 purified from conditioned media of vector-, GnT-III-, or GnT-V-MKN45 transfectants.** Purified laminin-332s, vector-Lm332 (*vector*), GnT-III-Lm332 (*GnT-III*), and GnT-V-Lm332 (*GnT-V*), were run on 4–7.5% gradient gels and 6% gels under nonreducing (*−ME*) and reducing conditions (*+ME*), respectively. After SDS-PAGE, separated proteins were stained with CBB (*A; CBB*) or transferred to the nitrocellulose membranes. Blotted proteins were probed with monoclonal antibodies against laminin α3 (LSαC3), β3 (kalinin B1), and γ2 (D4B5) chain (*B; I.B.*). *Ordinates* indicate molecular sizes in kDa of marker proteins and laminin chains.

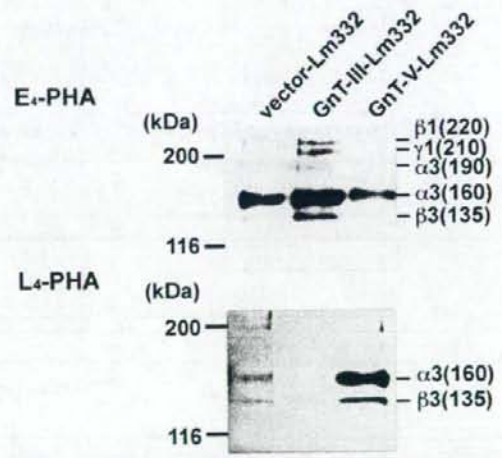

FIGURE 3. **Lectin blotting analysis of purified laminin-332s.** 100 ng of laminin-332s (vector-, GnT-III-, and GnT-V-Lm332) was separated on 6% SDS-PAGE gel and then blotted onto the nitrocellulose membranes. Blotted proteins were probed with E_4-PHA (*top*) and L_4-PHA (*bottom*) lectin. *Ordinates* indicate molecular sizes in kDa of marker proteins and laminin chains.

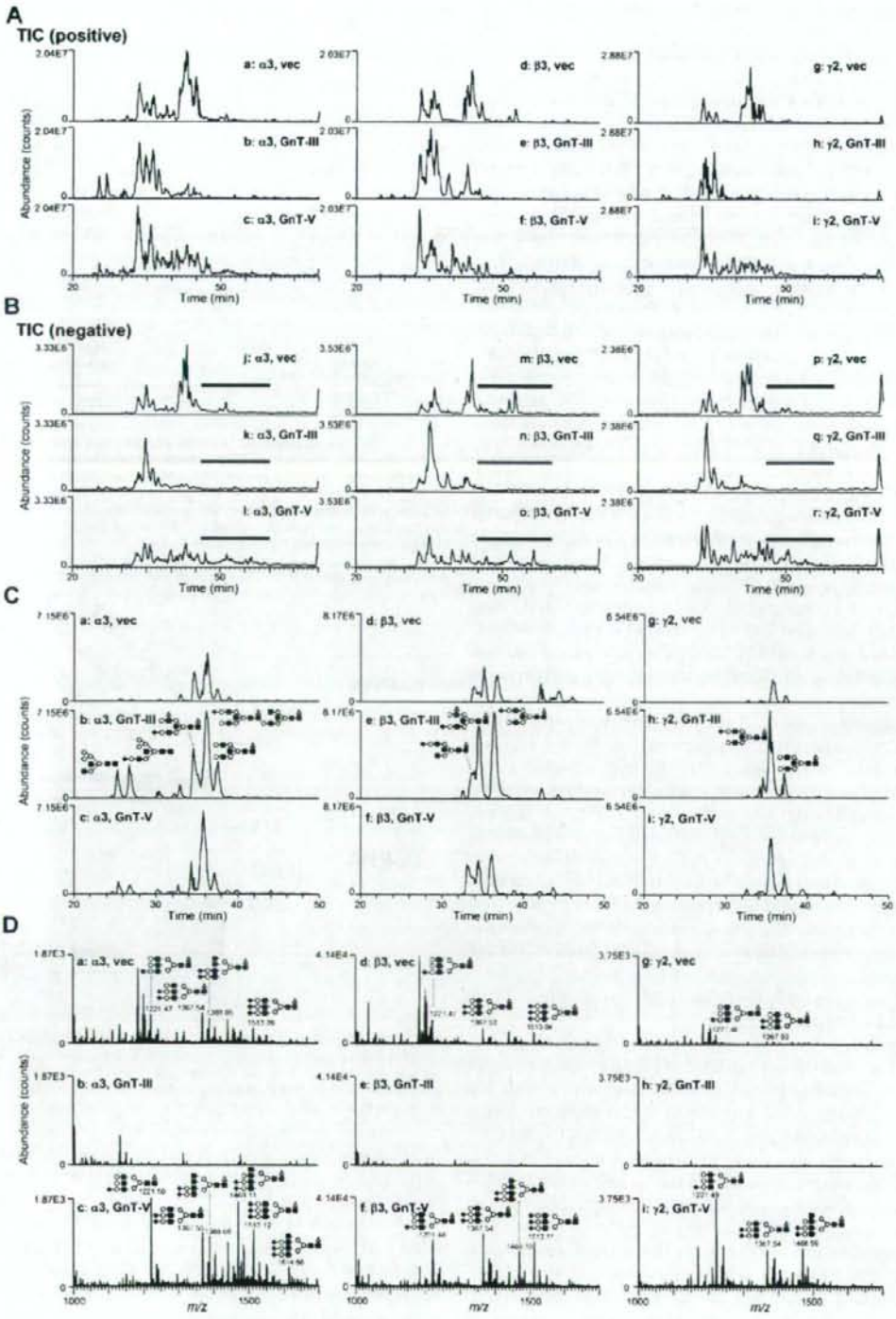

tion for 1 h at 37 °C, cell movement was monitored using time lapse video equipment (Carl Zeiss) for 8 h.

ELISA—The ELISA was as follows. The wells of a 96-well plate were coated with test proteins and then blocked with 1.2% BSA at room temperature for 1 h. The wells were washed with PBS containing 0.05% Tween 20 (washing buffer) three times and then incubated with primary antibody for 1 h at room temperature. Furthermore, the wells were washed with washing buffer three times and then incubated with secondary antibody coupled with biotin for 45 min at room temperature. Similarly, the wells were washed three times and incubated with alkaline phosphatase conjugated with avidin D for 45 min at room temperature. After five washes with washing buffer, the bound antibodies were quantified by their absorbance at 405 nm after incubation with *p*-nitrophenylphosphate disodium salt in 100 mM diethanolamine (pH 9.8) containing 0.24 mM $MgCl_2$.

Immunofluorescence Microscopy—A glass bottom dish (Asahi Techno Glass) was precoated with purified Lm332 and then blocked with 1% BSA for 1 h at 37 °C. 200 μl of the cell suspension (2×10^5 cells/ml) in growth medium were inoculated into each Lm332-precoated glass bottom dish. After incubation for 1 h, the cells were washed with PBS and then fixed with 4% (w/v) paraformaldehyde in PBS for 10 min. For permeabilization, the cells were treated with 0.2% (v/v) Triton X-100 in PBS. The fixed cells were blocked with 2% BSA in PBS for 1 h before staining with appropriate primary and secondary antibodies. Fluorescence images were obtained using a fluorescence microscope (Olympus, Tokyo) equipped with ×100/1.35 UPlan-Apochromat oil immersion objectives.

Statistical Analysis—Data are presented as mean ± S.D. Student's *t* test, with Microsoft Excel, was used to compare the two groups.

RESULTS

Characterization of GnT-III and GnT-V Transfectants—As a source for purification of Lm332 modified by GnT-III- or GnT-V-catalyzed glycosylation, we prepared GnT-III- and GnT-V-overexpressing MKN45 transfectants and also a vector-only transfectant to be used as a negative control as previously described (27). To check the changes in oligosaccharide structures for each transfectant, lectin blotting was performed against the cell lysates from those transfectants using E_4-PHA, which preferentially binds to bisecting GlcNAc residues in *N*-glycans or L_4-PHA, which preferentially binds to β1,6-branched GlcNAc residues (30). The blotting results showed that the GnT-III transfectant increased bisecting GlcNAc compared with the other two (Fig. 1*B*, *E_4-PHA*) but decreased GnT-V products (Fig. 1*B*, *L_4-PHA*), supporting the notion that GnT-III antagonizes the action of GnT-V for the modification of some target glycoproteins, such as α3β1 integrin (25). On the other hand, GnT-V overexpression had no effect on the GnT-III product level (Fig. 1*B*, *E_4-PHA*) but led to a strong increase of β1,6-branched GlcNAc in MKN45 cells (Fig. 1*B*, *L_4-PHA*). The immunoblotting using an anti-α-tubulin antibody showed that the amount of a loaded protein was almost the same among the three samples (Fig. 1*B*, *α-tubulin*).

Purification and Characterization of Lm332 from MKN45 Transfectants—To examine whether Lm332 could be modified by GnT-III or GnT-V to regulate its functions, we tried to purify Lm332 from the CM of vector-, GnT-III-, and GnT-V-MKN45 transfectants using a laminin α3 chain antibody (2B10) column. Purified Lm332 was run on 4–7.5% gradient gel and 6% gel for CBB staining and immunoblotting, respectively (Fig. 2). CBB staining under nonreducing conditions revealed two major bands at ~460 and 440 kDa, which correspond to the Lm332 forms with an unprocessed 150-kDa γ2 chain and with a processed 105-kDa γ2 chain, respectively (Fig. 2, *CBB, left*). SDS-PAGE under reducing conditions separated the Lm subunits. All purified Lm332s contained the three major bands of 160-, 150-, and 135-kDa proteins, which correspond to the processed α3 chain, the unprocessed γ2 chain, and the β3 chain, respectively (Fig. 2, *CBB, right*). In addition to those bands, there are three extra bands, which were larger than the 160-kDa processed α3 chain band. Mass spectrometry analysis showed that those bands are laminin β1, γ1, and an unprocessed α3 chain (190 kDa) (data not shown). A likely explanation is that this represented laminin-311 (Lm311; laminin-6), which is composed of α3, β1, and γ1 chains. Lm332 purified from GnT-III MKN45 transfectant (GnT-III-Lm332) contained slightly increased amounts of those extra bands rather than the Lm332 from vector MKN45 (vector-Lm332) and from GnT-V MKN45 transfectants (GnT-V-Lm332), suggesting that the processing of the α3 chain, but not the β3 and γ2 chains, could be affected by the addition of bisecting GlcNAc. The quantified band intensity upon CBB staining under reducing conditions showed that the ratio of β3 chain in Lm332 to β1 chain in Lm311 was 10:1 (data not shown). Under nonreducing conditions, it was difficult to find the bands corresponding to Lm332 with an unprocessed laminin α3 chain (490 kDa) and Lm311 (600 kDa). The compositions of the Lm332 chain were also confirmed by immunoblotting using each chain-specific antibody. Consistent with the results shown in CBB staining, GnT-III-Lm332 contained slightly more unprocessed α3 chains (190-kDa) than those of vector-Lm332 and GnT-V-Lm332 (Fig. 2, *I.B. α3*). By contrast, there were no differences between the 135-kDa β3 chain, the unprocessed 150-kDa γ2 chain, and the processed 105-kDa γ2 chain among three Lm332s (Fig. 2, *I.B. β3* and *γ2*).

FIGURE 4. **Analysis of *N*-glycan structures of purified laminin-332s by LC/MS^n.** Total ion chromatograms (*TICs*) obtained by single mass scans of *N*-glycans extracted from the gel separated Lm332 subunits (*left*, α3; *middle*, β3; *right*, γ2) of vec-Lm332 (*top, vec*), GnT-III-Lm332 (*middle, GnT-III*), and GnT-V-Lm332 (*bottom, GnT-V*) in positive (*A*) and negative (*B*) ion modes. *C*, extracted ion chromatograms of representative bisected *N*-glycans acquired by single mass scans. The extracted ion chromatogram of α3 subunit is shown at *m/z* 822.3, 915.9, 996.9, 1048.9, 1,142.4, and 1,215.5 (*a*, vector; *b*, GnT-III-Lm332; *c*, GnT-V-Lm332). The extracted ion chromatogram of β3 subunit is shown at *m/z* 1,061.4, 1,142.4, and 1,215.5 (*d*, vector; *e*, GnT-III-Lm332; *f*, GnT-V-Lm332). The extracted ion chromatogram of γ2 subunit is shown at *m/z* 1,142.4 and 996.9 (*g*, vector; *h*, GnT-III-Lm332; *i*, GnT-V-Lm332). The *insets* show deduced structures (*gray triangle*, fucose; *open circle*, galactose; *gray circle*, mannose; *black square*, *N*-acetylglucosamine; *black diamond*, *N*-acetylneuraminic acid). *D*, integrated mass spectra (*m/z* 1,000–1,700) acquired at elution positions indicated by *boldface lines* in total ion chromatograms in negative ion mode (Fig. 4*B*) (*left*, α3; *middle*, β3; *right*, γ2; *top*, vector; *middle*, GnT-III-Lm332; *bottom*, GnT-V-Lm332). The *insets* show deduced structure (*gray triangle*, fucose; *open circle*, galactose; *gray circle*, mannose; *black square*, *N*-acetylglucosamine; *black diamond*, *N*-acetylneuraminic acid).

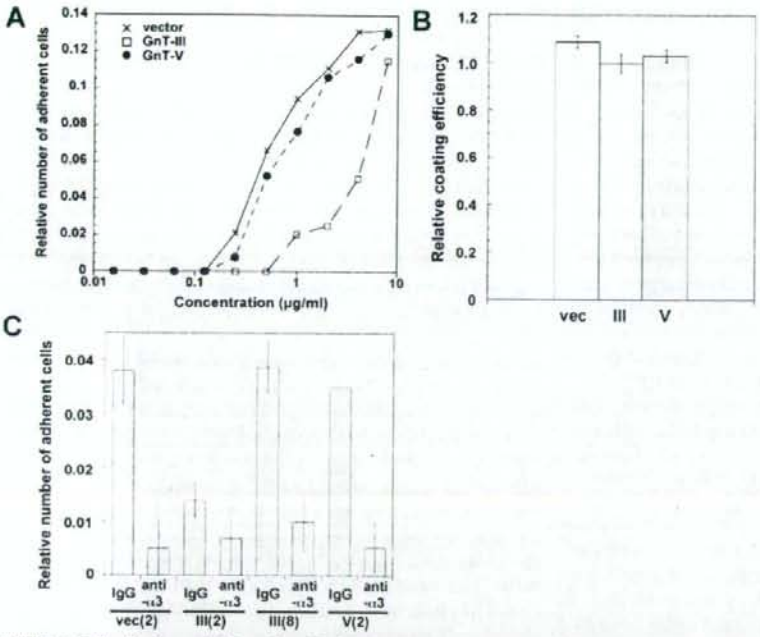

FIGURE 5. **Cell adhesion activities of purified laminin-332s.** *A*, cell adhesion activities of vector-Lm332 (*crosses*), GnT-III-Lm332 (*open squares*), and GnT-V-Lm332 (*closed circles*). The 96-well plates were coated with the indicated concentrations of each Lm332. After 1.2% BSA blocking, Lm332-null keratinocytes suspended in supplement-free keratinocyte medium were plated to each well and incubated for 20 min. Each point represents the mean of triplicate assays. Other experimental conditions are described in "Experimental Procedures." *B*, 2 μg/ml Lm332s were coated to the 96-well ELISA plates at 4 °C overnight. After blocking those wells with 1.2% BSA, coating efficiency of three kinds of Lm332s was estimated by ELISA using anti-laminin γ2 chain antibody. *C*, inhibitory effects of function blocking antibody against integrin α3 (*anti-α3*) or control mouse IgG (*IgG*) on cell adhesion of Lm332-null keratinocytes to different kinds of Lm332s. The *numbers in parentheses* indicate the concentrations for Lm332 (μg/ml). Each *bar* represents the mean ± S.D. of triplicate assays.

To establish whether Lm332 was modified by GnT-III or GnT-V, lectin blotting using E_4-PHA and L_4-PHA lectin was performed against three purified Lm332s. A comparison of bands corresponding to α3 and β3 chains among three purified Lm332s indicated that increased GnT-III and GnT-V products presented on GnT-III-Lm332 and GnT-V-Lm332, respectively (Fig. 3). Upon E_4-PHA lectin blotting against GnT-III-Lm332, bisecting GlcNAc was added to β1 and γ1 chains as well as to the unprocessed α3A chain (Fig. 3, *E_4-PHA*). To ascertain the *N*-glycan structures on Lm332 subunits directly, we also performed liquid chromatography/multiple-stage mass spectrometry (LC/MS^n) analyses. Each subunit of Lm332 was separated by SDS-PAGE under reducing conditions, and *N*-glycans in each subunit were released by in-gel digestion with peptide:*N*-glycanase F. The oligosaccharides were extracted from the gel and subjected to LC/MS^n as described under "Experimental Procedures." Total ion chromatograms were acquired by single mass scans (m/z 450–2,000) in positive (Fig. 4*A*) and negative (Fig. 4*B*) ion modes, respectively. Structures of *N*-glycans in major peaks were deduced from m/z values of protonated molecules acquired by Fourier transform ion cyclotron resonance-MS and fragment ions in MS^n spectra. Additional bisected *N*-glycans were confirmed based on the fragment ions at m/z 792 ([HexNAc-Hex-HexNAc-HexNAc-OH + H]$^+$) and m/z 938 ([HexNAc-Hex-HexNAc-(dHex-)HexNAc-OH + H]$^+$) in MS/MS and MS/MS/MS spectra. The extracted ion chromatograms of representative bisected *N*-glycans were acquired by single mass scans, and the structures in each peak were deduced (Fig. 4*C*). The peaks of the bisected *N*-glycans from all three subunits of GnT-III-Lm332 (Fig. 4, *C*, *b*, *e*, and *h*) were more intense than those from both the vec-Lm332 (Fig. 4*C*, *a*, *d*, and *g*) and GnT-V-Lm332 (Fig. 4*C*, *c*, *f*, and *i*). We also examined the β1,6-GlcNAc structures on all subunits of three Lm332s (Fig. 4*D*). The majority of *N*-glycans in all three subunits of vec-Lm332 (Fig. 4*D*, *a*, *d*, and *g*) and GnT-V-Lm332 (Fig. 4*D*, *c*, *f*, and *i*) were sialylated triantennary, whereas few triantennary forms were found in those of GnT-III-Lm332 (Fig. 4*D*, *b*, *e*, and *h*). These results, taken together, suggest that all subunits of Lm332 were modified by GnT-III and GnT-V, and they also support the notion that introduction of GnT-III inhibits GnT-V products.

Comparison of GnT-III- and GnT-V-Lm332-induced Cell Adhesion Activities—The localization of laminin isoform can be defined by the laminin α subunit, which is expressed in a tissue-specific distribution. For example, the laminin α2 chain containing laminin and the laminin α4 chain containing laminin localizes to the skeletal muscle and blood vessels, respectively. On the other hand, Lm332, which includes the laminin α3 chain, extensively localizes to the skin and stratified squamous tissues *in vivo*. To understand the biological activities of Lm332, we used the keratinocyte as a model cell, since Lm332 is a major component of keratinocyte extracellular matrix (ECM).

Lm332 promotes keratinocyte or other epithelial cell spreading and adhesion more effectively than other ECM proteins, such as collagen, fibronectin, and Lm111 (31). To examine the effect of GnT-III and GnT-V modification on Lm332 activities, we tried to perform a cell adhesion assay among three Lm332s. Generally, it is difficult to measure the biological functions of other ECMs in Lm332-expressing cells because the endogenous Lm332 strongly affects the experimental results. In order to prevent this, we used purified Lm332 and the Lm332-null keratinocytes established from patients with genetic mutations of the laminin β3 chain. Cell adhesion activity of GnT-V-Lm332 toward Lm332-null keratinocytes was similar to that of vector-Lm332 but was decreased in GnT-III-Lm332 (Fig. 5*A*). Cells displayed round morphology and formed filopodia around cells

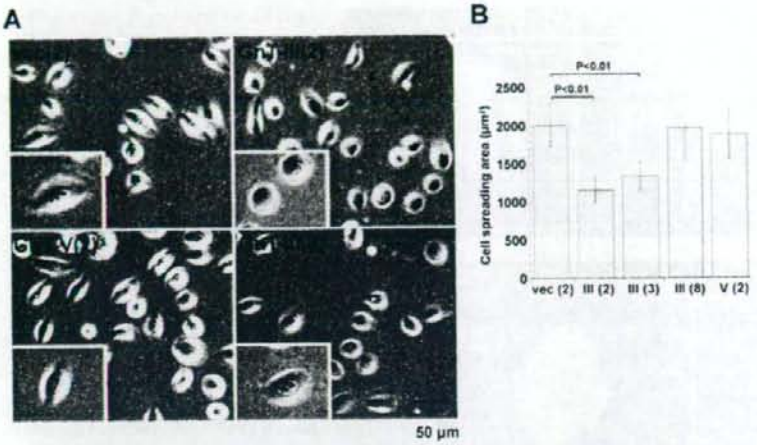

FIGURE 6. **Effects of *N*-glycosylation on laminin-332-mediated cell spreading.** Lm332-null keratinocytes were plated to the wells, which were precoated with vector-Lm332 (*vec*), GnT-III-Lm332 (*GnT-III*), and GnT-V-Lm332 (*GnT-V*), and then incubated for 1.5 h. *A*, cell morphology of Lm332-null keratinocytes on each substrate. *Inset*, a representative cell morphology. *B*, the cell spreading area was calculated using computer software (AxioVision). The *numbers* in *parentheses* are the concentrations for Lm332 (μg/ml). Each *bar* represents the mean ± S.D. of triplicate assays.

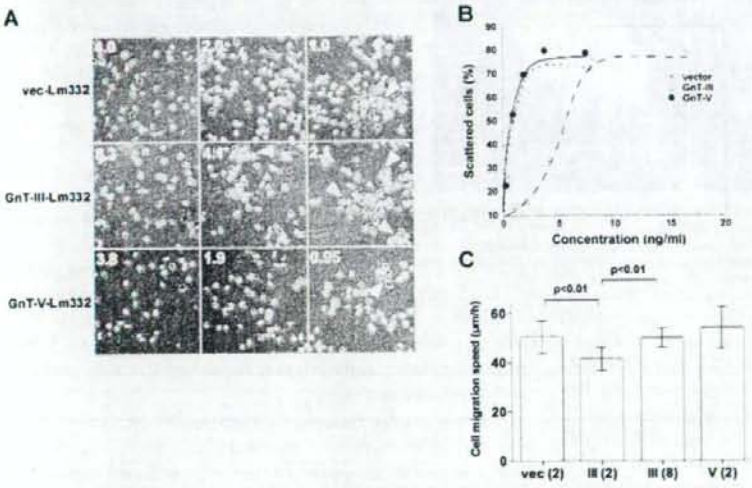

FIGURE 7. **Cell scattering and migration activities of *N*-glycosylated laminin-332s.** BLR cells were incubated with the indicated concentrations of Lm332s. After 40 h of incubation, cells were fixed and stained with crystal violet for observing cell scattering. *A*, cell morphology of BLR cells in each indicated condition. The *numbers* on the *left* are the concentrations for Lm332 (ng/ml) in cell culture medium. The *arrowheads* indicate the cluster of cells. *B*, scattered cells were counted and indicated as a percentage against total number of the cells. *Crosses*, vector-Lm332; *open squares*, GnT-III-Lm332; *closed circles*, GnT-V-Lm332. *C*, effects of vector-Lm332 (*vec*), GnT-III-Lm332 (*III*), and GnT-V-Lm332 (*V*) on migration of Lm332-null keratinocytes. The migration on each substrate was monitored by time lapse microscopy for 8 h. Each *bar* represents the mean ± S.D. of the migration speeds of nine cells. The *numbers* in *parentheses* are the concentrations for Lm332 (μg/ml). Other experimental conditions are under "Experimental Procedures."

plated on culture dishes coated with 2 μg/ml GnT-III-Lm332 (Fig. 6*A*). In contrast, cells cultured on 2 μg/ml vector-Lm332 or GnT-V-Lm332 exhibited well spreading morphology with lamellipodia (Fig. 6*A*). The effect of 8 μg/ml GnT-III-Lm332 on cell morphology and spreading was similar to those of 2 μg/ml vector-Lm332 and GnT-V-Lm332 (Fig. 6, *A* and *B*). To ascertain whether GnT-III modification on Lm332 caused a decrease in its binding to the plates, coating efficiency was checked by ELISA using laminin γ2 chain monoclonal antibody (D4B5). As a result, there were no differences in coating efficiencies among the three Lm332s (Fig. 5*B*). Lm332 mainly binds integrin α3β1 and α6β4 as a cell surface receptor (6, 31). To ensure whether *N*-glycosylation affects the integrin binding function of Lm332, an inhibition assay was done using integrin α3 (P1B5) and α6 (GoH3) inhibitory antibodies. In all conditions, the anti-α3 antibody treatment completely diminished cell attachment toward the Lm332 substrate (Fig. 5*C*). Anti-α6 antibody (GoH3) (data not shown) as well as control IgG did not show inhibitory effects on the cell adhesion toward all Lm332 substrates. The possibility still remained that the effects of GnT-III-Lm332 could be due to the small amount of contaminating non-Lm332 subunits. To exclude this possibility, we attempted the cell adhesion assay using immunocaptured Lm332s to the plates with the laminin γ2 antibody (D4B5). A similar result to that in Fig. 5*A* was obtained in the experiment (data not shown). These results suggest that GnT-III products on Lm332 decreased its cell adhesion and cell spreading activities but had no influence on the integrin usage.

Effects of GnT-III and GnT-V Modification of Lm332 on Cell Scattering and Migration Activities—Cell scattering, which represents epithelial cell dissociation, is a well known Lm332 function (10, 11). To test whether GnT-III or GnT-V modification of Lm332 can influence its cell scattering activity, we investigated the scattering morphology using a Buffalo rat liver epithelial cell line (BLR cells), which is sensitive to the scattering activity of Lm332 (10). When the final concentration of vector-Lm332 at 2.0 ng/ml was added to the culture medium of BLR cells, more than 70% of the BLR cells markedly exhibited scattering morphology, as shown in Fig. 7*A*. GnT-V-Lm332 showed similar scattering activity to vector-Lm332. In contrast, GnT-III-Lm332 at 2.0 ng/ml did not

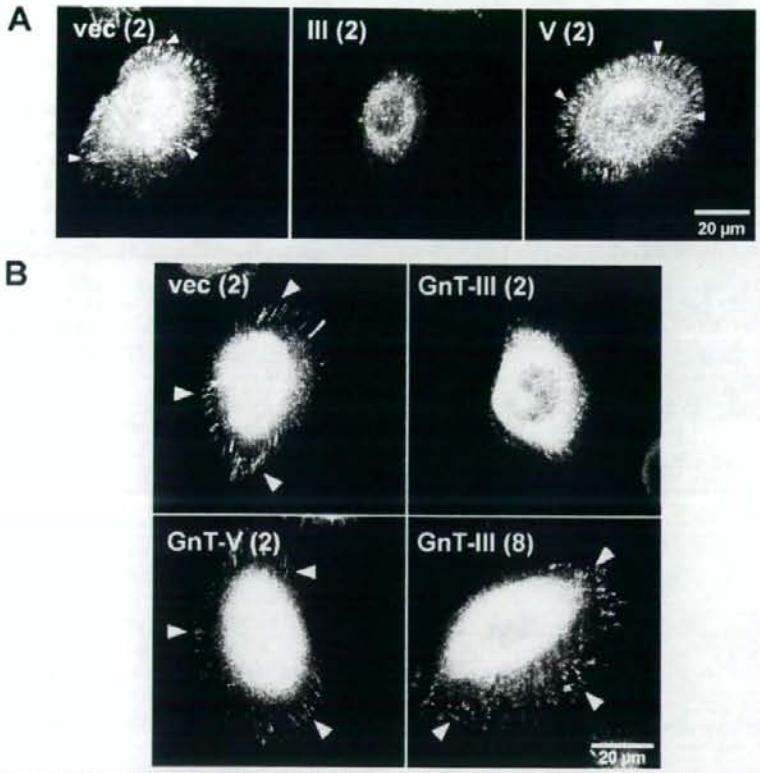

FIGURE 8. **Effects of *N*-glycosylation on laminin-332-mediated $\alpha3\beta1$ integrin association and focal contact formation.** For visualizing $\alpha3$ integrin (*A*) and paxillin (*B*), Lm332-null keratinocytes were plated on the indicated Lm332s and then incubated for 1.5 h. After fixation, cells were stained with appropriate primary and secondary antibodies. The *numbers* in *parentheses* are the concentrations for Lm332 (μg/ml). The *arrowheads* indicate $\alpha3\beta1$ integrin clustering (*A*) and focal contacts (*B*).

show scattering activity. The concentration for the half-maximal scattering activity (ED_{50}) was ~0.5 ng/ml for vector-Lm332 and GnT-V-Lm332 but 5.0 ng/ml for GnT-III-Lm332 (Fig. 7*B*). We also compared cell migration activity among three Lm332s. When coated at 2 μg/ml, GnT-III-Lm332 showed decreased cell migration activity compared with vec-Lm332 and GnT-V-Lm332. However, when GnT-III-Lm332 was coated at 8 μg/ml for each plate, the activity was recovered to a level similar to those of 2 μg/ml vec-Lm332 and GnT-V-Lm332 (Fig. 7*C*). These results strongly support the notion that remodeling of *N*-glycans plays an important biological role.

Effects of N-Glycosylation on Lm332-mediated $\alpha3\beta1$ Integrin Association and Focal Complex Formation—Upon cell binding to ECM proteins, integrins undergo conformational changes, and their cytoplasmic domains interact through linker molecules, such as paxillin with the actin cytoskeleton and with signaling proteins (32). Furthermore, ECM induces integrin clustering, which can amplify various cell signaling from ECM (33). To clarify the reason why GnT-III-Lm332 showed lower activities than either vec-Lm332 or GnT-V-Lm332, we examined whether the modification of Lm332 by GnT-III or GnT-V affects the $\alpha3\beta1$ integrin clustering or focal contact formation using fluorescence microscopy. Integrin $\alpha3$ clustering (Fig. 8*A*) and focal contacts (Fig. 8*B*, paxillin) were distinctly observed in those cells cultured on 2 μg/ml vec-Lm332 as well as on GnT-V-Lm332 but not those cultured on GnT-III-Lm332. When cells were plated on 8 μg/ml GnT-III-Lm332, the focal contacts were clearly visualized by paxillin staining (Fig. 8*B*). These results suggest that modification of Lm332 by bisecting GlcNAc reduces the efficiency of integrin $\alpha3\beta1$ clustering, which may in turn suppress focal contact formation.

DISCUSSION

In this study, we intensively investigated the effects of *N*-glycosylation on the biological functions of Lm332. GnT-III-Lm332 and GnT-V-Lm332 were modified with bisecting GlcNAc and $\beta1,6$-branched GlcNAc, respectively. Our further analyses demonstrated that introduction of bisecting GlcNAc to Lm332 decreased its cell spreading, adhesion, and scattering activities as well as its migration activity. Although three kinds of Lm332s showed no significant differences concerning integrin $\alpha3\beta1$ binding function, GnT-III-Lm332 decreased $\alpha3\beta1$ integrin clustering and the resultant focal contact formation.

In some cancer tissues, overexpression of GnT-V was observed by immunohistochemistry (20, 34, 35). Deficient GnT-V expression suppressed tumor growth and metastasis in animal models (21). Furthermore, Patridge *et al.* (36) reported that modification of growth factor receptors, such as epidermal growth factor and transforming growth factor-β receptors, with *N*-glycans using poly-*N*-acetyllactosamine produced by GnT-V caused preferential receptor binding to galectins, resulting in formation of a lattice that opposes constitutive endocytosis. These data suggest that GnT-V affects the cancer by promoting cell motility and changing the stability for growth factor receptors at the cell surface. Ly6 family member C4.4A can bind to Lm332, and its association of galectin-3 influences Lm332 adhesion (37). In addition, galectin-3-dependent oligomerization potentiates NG2-mediated activation of $\alpha3\beta1$ integrin (38). Recently, we found that galectin-3 could bind to

Lm332.[3] It is possible that galectin-3 links GnT-V-modified-Lm332 and $\alpha3\beta1$ integrin as well as growth factor receptors via poly-*N*-acetyllactosamine, resulting in the clustering and activation of the Lm332-$\alpha3\beta1$ integrin-growth factor receptor complexes as well as causing resistance to their endocytosis. In contrast, modification of GnT-III suppresses further processing with branching enzymes, such as GnT-V, and elongation of *N*-glycans. Our previous study showed that the increase of GnT-V products on integrin $\alpha3$ promoted cell migration on Lm332, whereas introduction of bisecting GlcNAc into the integrin $\alpha3$ subunit resulted in a decrease of $\alpha3\beta1$ integrin-mediated cancer cell motility by inhibition of $\beta1,6$-branched GlcNAc modification on the $\alpha3$ integrin subunit (25). Lm332, which is a specific substrate for $\alpha3\beta1$ integrin, promotes cell motility during wound healing and tumor progression (11, 12). In contrast to integrin $\alpha3\beta1$, although introduction of bisecting GlcNAc significantly reduced the activities of Lm332, the modification of GnT-V does not affect the activities of Lm332 compared with the activities of vector-Lm332. It could be argued that intrinsic GnT-V-mediated glycosylation is enough for occupation of functional *N*-glycosylation sites of vector-Lm332 as well as of GnT-V-Lm332. As shown in both Fig. 3 and Fig. 4, $\beta1,6$-branched GlcNAc was expressed on vector-Lm332. Actually, we found that the integrin $\alpha5$ subunit has fewer important *N*-glycosylation sites for its biological functions and expression on its cell surface, although it has 14 potential *N*-glycosylation sites (39).

Matsui *et al.* (40) showed that loss of *N*-glycosylation was not necessary for Lm332 assembly and secretion. The present study consistently showed that the modification of either GnT-III or GnT-V had no effect on Lm332 assembly and secretion. However, GnT-III-Lm332 was slightly resistant to the proteolytic processing of the laminin $\alpha3$ subunit compared with the vector-Lm332 and GnT-V-Lm332. A slight increase in unprocessed laminin $\alpha3$ subunits (190-kDa form) might result in the up-regulation of Lm311 formation, since laminin $\beta1$ and $\gamma1$ preferentially assembled with the unprocessed $\alpha3$ chain rather than with the processed $\alpha3$ chain (41). These results may also suggest that *N*-glycosylation affects trimeric formation among laminin subunits *in vivo*. In this study, since purified GnT-III-Lm332 contained a very small amount of the unprocessed $\alpha3$ chain, the effect of those Lms in purified GnT-III-Lm332 was thought to be negligible. Moreover, the activities of Lm311 and Lm332 with the unprocessed form of the $\alpha3$ chain are not so different from those of Lm332 with the processed $\alpha3$ subunit (160-kDa form) (16, 41), compared with the differences between GnT-III-Lm332 and either vector-Lm332 or GnT-V-Lm332. Therefore, the decreased activities of GnT-III-Lm332 were mainly caused by the addition of bisecting GlcNAc to Lm332. In previous studies, Lm311 slightly stimulated cell spreading in the presence of a low concentration of Lm332, whereas Lm311 showed no cell spreading activities by itself (41). Although it is not the case for this study, the clarification of the molecular mechanism underlying the association of GnT-III-Lm332 with Lm311 could be a very interesting theme. Moreover, since syndecan-1, -2, and -4 can bind to the G4-G5 domain in the unprocessed laminin $\alpha3$ chain (42, 43), we cannot definitely exclude the effect of syndecan on Lm332 activities, although the vast majority of Lm332 was processed (without the G4-G5 domain), compared with unprocessed Lm332 (with the G4-G5 domain) in this study. A previous study (44) showed that deglycosylation of recombinant Lm332 containing the heterotrimeric, C-terminal part of the coiled-coil domain and G domains did not affect its binding to integrin $\alpha3\beta1$. However, we found that the addition of bisecting GlcNAc to Lm332 diminished Lm332-mediated $\alpha3\beta1$ integrin clustering and the subsequent cell adhesion, spreading and scattering as well as the migration induced by Lm332. It is reasonable to assume that galectin-3 can link molecules via poly-*N*-acetyllactosamine, because galectin-3 binding to GnT-III-Lm332 is probably much less than its binding to either vector- or GnT-V-Lm332. Details of the molecular mechanism in play here will require further study.

In the basement membranes of the skin and of other tissues, there are many components, such as type IV collagen, nidogens, proteoglycans, agrin, and laminin-511 (Lm511; laminin-10), that contribute to structure and receptor interactions. Since most ECM proteins are glycoproteins, alteration of carbohydrates could change carbohydrate/carbohydrate or carbohydrate/protein interactions in the basement membrane, which presumably affects functional activities of diverse ECM. To understand how carbohydrate modifications affect the skin and other tissues, therefore, the analysis of carbohydrate functions of individual or combined ECM proteins is quite important. This will be further addressed in future studies.

In conclusion, this study reports for the first time that Lm332 can be modified by both GnT-III and GnT-V, resulting in the regulation of cell spreading, adhesion, scattering, and migration activities induced by Lm332. In addition, *N*-glycosylation of Lm332 can influence the proteolytic processing of laminin subunits and $\alpha3\beta1$ integrin clustering. Given the importance of Lm332 and the dynamic changes in *N*-glycosylation during tumor formation and cancer metastasis, *N*-glycan could represent a new therapeutic target.

Acknowledgment—We thank Dr. M. Peter Marinkovich (Stanford University) for critical reading of the manuscript.

[3] Y. Kariya and J. Gu, unpublished data.

REFERENCES

1. Colognato, H., and Yurchenco, P. D. (2000) *Dev. Dyn.* **218,** 213–234
2. Fujiwara, S., Shinkai, H., Deutzmann, R., Paulsson, M., and Timpl, R. (1988) *Biochem. J.* **252,** 453–461
3. Dean, I. W., III, Chandrasekaran, S., and Tanzer, M. L. (1990) *J. Biol. Chem.* **265,** 12553–12562
4. Green, T. L., Hunter, D. D., Chan, W., Merlie, J. P., and Sanes, J. R. (1992) *J. Biol. Chem.* **267,** 2014–2022
5. Howe, C. C. (1984) *Mol. Cell Biol.* **4,** 1–7
6. Carter, W. G., Ryan, M. C., and Gahr, P. J. (1991) *Cell* **65,** 599–610
7. Ryan, M. C., Christiano, A. M., Engvall, E., Wewer, U. M., Miner, J. H., Sanes, J. R., and Burgeson, R. E. (1996) *Matrix Biol.* **15,** 369–381
8. Kariya, Y., Tsubota, Y., Hirosaki, T., Mizushima, H., Puzon-McLaughlin, W., Takada, Y., and Miyazaki, K. (2003) *J. Cell Biochem.* **88,** 506–520
9. Nguyen, B. P., Gil, S. G., and Carter, W. G. (2000) *J. Biol. Chem.* **275,** 31896–31907

10. Kariya, Y., and Miyazaki, K. (2004) *Exp. Cell Res.* **297,** 508–520
11. Miyazaki, K. (2006) *Cancer Sci.* **97,** 91–98
12. Marinkovich, M. P. (2007) *Nat. Rev. Cancer* **7,** 370–380
13. Giannelli, G., Falk-Marzillier, J., Schiraldi, O., Stetler-Stevenson, W. G., and Quaranta, V. (1997) *Science* **277,** 225–228
14. Veitch, D. P., Nokelainen, P., McGowan, K. A., Nguyen, T. T., Nguyen, N. E., Stephenson, R., Pappano, W. N., Keene, D. R., Spong, S. M., Greenspan, D. S., Findell, P. R., and Marinkovich, M. P. (2003) *J. Biol. Chem.* **278,** 15661–15668
15. Koshikawa, N., Giannelli, G., Cirulli, V., Miyazaki, K., and Quaranta, V. (2000) *J. Cell Biol.* **148,** 615–624
16. Tsubota, Y., Yasuda, C., Kariya, Y., Ogawa, T., Hirosaki, T., Mizushima, H., and Miyazaki, K. (2005) *J. Biol. Chem.* **280,** 14370–14377
17. Cummings, R. D., Trowbridge, I. S., and Kornfeld, S. (1982) *J. Biol. Chem.* **257,** 13421–13427
18. Shoreibah, M., Perng, G. S., Adler, B., Weinstein, J., Basu, R., Cupples, R., Wen, D., Browne, J. K., Buckhaults, P., and Fregien, N. (1993) *J. Biol. Chem.* **268,** 15381–15385
19. Dennis, J. W., and Laferte, S. (1989) *Cancer Res.* **49,** 945–950
20. Handerson, T., and Pawelek, J. M. (2003) *Cancer Res.* **63,** 5363–5369
21. Granovsky, M., Fata, J., Pawling, J., Muller, W. J., Khokha, R., and Dennis, J. W. (2000) *Nat. Med.* **6,** 306–312
22. Gu, J., Nishikawa, A., Tsuruoka, N., Ohno, M., Yamaguchi, N., Kangawa, K., and Taniguchi, N. (1993) *J. Biochem. (Tokyo)* **113,** 614–619
23. Schachter, H. (1986) *Biochem. Cell Biol.* **64,** 163–181
24. Yoshimura, M., Nishikawa, A., Ihara, Y., Taniguchi, S., and Taniguchi, N. (1995) *Proc. Natl. Acad. Sci. U. S. A.* **92,** 8754–8758
25. Zhao, Y., Nakagawa, T., Itoh, S., Inamori, K., Isaji, T., Kariya, Y., Kondo, A., Miyoshi, E., Miyazaki, K., Kawasaki, N., Taniguchi, N., and Gu, J. (2006) *J. Biol. Chem.* **281,** 32122–32130
26. Fujiwara, H., Kikkawa, Y., Sanzen, N., and Sekiguchi, K. (2001) *J. Biol. Chem.* **276,** 17550–17558
27. Ihara, S., Miyoshi, E., Ko, J. H., Murata, K., Nakahara, S., Honke, K., Dickson, R. B., Lin, C. Y., and Taniguchi, N. (2002) *J. Biol. Chem.* **277,** 16960–16967
28. Kuster, B., Wheeler, S. F., Hunter, A. P., Dwek, R. A., and Harvey, D. J. (1997) *Anal. Biochem.* **250,** 82–101
29. Itoh, S., Kawasaki, N., Hashii, N., Harazono, A., Matsuishi, Y., Hayakawa, T., and Kawanishi, T. (2006) *J. Chromatogr. A.* **1103,** 296–306
30. Cummings, R. D., and Kornfeld, S. (1982) *J. Biol. Chem.* **257,** 11230–11234
31. Rousselle, P., and Aumailley, M. (1994) *J. Cell Biol.* **125,** 205–214
32. Hughes, P. E., and Pfaff, M. (1998) *Trends Cell Biol.* **8,** 359–364
33. Carman, C. V., and Springer, T. A. (2003) *Curr. Opin. Cell Biol.* **15,** 547–556
34. Fernandes, B., Sagman, U., Auger, M., Demetrio, M., and Dennis, J. W. (1991) *Cancer Res.* **51,** 718–723
35. Murata, K., Miyoshi, E., Kameyama, M., Ishikawa, O., Kabuto, T., Sasaki, Y., Hiratsuka, M., Ohigashi, H., Ishiguro, S., Ito, S., Honda, H., Takemura, F., Taniguchi, N., and Imaoka, S. (2000) *Clin. Cancer Res.* **6,** 1772–1777
36. Partridge, E. A., Le Roy, C., Di Guglielmo, G. M., Pawling, J., Cheung, P., Granovsky, M., Nabi, I. R., Wrana, J. L., and Dennis, J. W. (2004) *Science* **306,** 120–124
37. Paret, C., Bourouba, M., Beer, A., Miyazaki, K., Schnolzer, M., Fiedler, S., and Zoller, M. (2005) *Int. J. Cancer* **115,** 724–733
38. Fukushi, J., Makagiansar, I. T., and Stallcup, W. B. (2004) *Mol. Biol. Cell* **15,** 3580–3590
39. Isaji, T., Sato, Y., Zhao, Y., Miyoshi, E., Wada, Y., Taniguchi, N., and Gu, J. (2006) *J. Biol. Chem.* **281,** 33258–33267
40. Matsui, C., Wang, C. K., Nelson, C. F., Bauer, E. A., and Hoeffler, W. K. (1995) *J. Biol. Chem.* **270,** 23496–23503
41. Hirosaki, T., Tsubota, Y., Kariya, Y., Moriyama, K., Mizushima, H., and Miyazaki, K. (2002) *J. Biol. Chem.* **277,** 49287–49295
42. Utani, A., Nomizu, M., Matsuura, H., Kato, K., Kobayashi, T., Takeda, U., Aota, S., Nielsen, P. K., and Shinkai, H. (2001) *J. Biol. Chem.* **276,** 28779–28788
43. Okamoto, O., Bachy, S., Odenthal, U., Bernaud, J., Rigal, D., Lortat-Jacob, H., Smyth, N., and Rousselle, P. (2003) *J. Biol. Chem.* **278,** 44168–44177
44. Kunneken, K., Pohlentz, G., Schmidt-Hederich, A., Odenthal, U., Smyth, N., Peter-Katalinic, J., Bruckner, P., and Eble, J. A. (2004) *J. Biol. Chem.* **279,** 5184–5193

Journal of Chromatography B, 869 (2008) 20–30

Contents lists available at ScienceDirect

Journal of Chromatography B

journal homepage: www.elsevier.com/locate/chromb

Simultaneous glycosylation analysis of human serum glycoproteins by high-performance liquid chromatography/tandem mass spectrometry

Akira Harazono[a,*], Nana Kawasaki[a,b], Satsuki Itoh[a], Noritaka Hashii[a], Yukari Matsuishi-Nakajima[a,b], Toru Kawanishi[a], Teruhide Yamaguchi[a]

[a] Division of Biological Chemistry and Biologicals, National Institute of Health Sciences, 1-18-1 Kami-yoga, Setagaya-Ku, Tokyo 158-8501, Japan
[b] Core Research for Evolutional Science and Technology (CREST) of Japan Science and Technology Agency (JST), Kawaguchi Center Building, 4-1-8 Hon-cho, Kawaguchi, Saitama 332-0012, Japan

ARTICLE INFO

Article history:
Received 19 December 2007
Accepted 5 May 2008
Available online 10 May 2008

Keywords:
Glycosylation analysis
Human serum
Glycopeptide
LC/MS
LC/MS/MS
Immunoglobulin G
Haptoglobin
Transferrin
Ceruloplasmin

ABSTRACT

Changes in the glycosylation of some serum proteins are associated with certain diseases. In this study, we performed simultaneous site-specific glycosylation analysis of abundant serum glycoproteins by LC/Qq-TOF MS of human serum tryptic digest, the albumin of which was depleted. The glycopeptide peaks on the chromatogram were basically assigned by database searching with modified peak-list text files of MS/MS spectra and then based on mass differences of glycan units from characterized glycopeptides. Glycopeptide of IgG, haptoglobin and ceruloplasmin were confirmed by means of a comparison of their retention times and *m/z* values with those obtained by LC/MS of commercially available glycoproteins. Mass spectrometric carbohydrate heterogeneity in the assigned glycopeptides was analyzed by an additional LC/MS. We successfully demonstrated site-specific glycosylation of 23 sites in abundant serum glycoproteins.

1. Introduction

Glycosylation of proteins is a common post-translational modification of proteins [1], and most proteins in serum are glycosylated [2]. Changes in the oligosaccharide moieties of certain serum glycoproteins are associated with human diseases. Oligosaccharides lacking galactose residues in immunoglobulin G (IgG) are increased in rheumatoid arthritis [3,4] and Crohn's syndrome [5]. Congenital disorders of glycosylation (CDG) are genetic disorders in the N-linked glycosylation processing pathway [6], and can be diagnosed by glycosylation analysis of serum glycoproteins [7], such as transferrin and haptoglobin. Significant increases in fucose levels and oligosaccharide branches in haptoglobin have been found to be associated with ovarian cancer [8,9], lung cancer [10–12], pancreatic cancer [13] and hepatocellular carcinoma [14]. Changes in glycosylation are also found in acute-phase proteins, such as alpha-1-acid glycoprotein and ceruloplasmin, in lung cancer [15]. These findings suggest the potential of the glycosylation analysis of serum glycoproteins in diagnosis of some diseases and an investigation of new biomarkers. At present the glycosylation of each protein is examined individually, therefore simultaneous analysis of serum glycoproteins has been required for rapid diagnosis with a limited amount of sample.

Mass spectrometry (MS) is known as a powerful tool for the glycosylation analysis of serum proteins. For the glycosylation analysis of serum glycoproteins, the enrichment of glycopeptides by lectin-affinity or hydrophilic chromatography is useful due to their low ionization efficiency, ionization suppression effects, and microheterogeneity [16–19]. There are still concerns about the loss of some glycopeptides during the preparation procedure, biased recoveries toward certain glycan structures, and low reproducibility of recovery. Liquid chromatography/mass spectrometry (LC/MS) is effective for the separation of glycopeptides and for the simultaneous glycosylation analysis.

Abbreviations: ESI, electrospray ionization; Fuc, fucose; GlcNAc, N-acetylglucosamine; Hex, hexose; HexNAc, N-acetylhexosamine; HPLC, high-performance liquid chromatography; IgG, immunoglobulin G; MS, mass spectrometry; MS/MS, tandem mass spectrometry; NeuAc, N-acetylneuraminic acid; Qq-TOF, quadrupole–quadrupole time-of-flight mass spectrometry; TIC, total ion chromatogram; EIC, extracted ion chromatogram.

* Corresponding author. Tel.: +81 3 3700 9074; fax: +81 3 3700 9084.
E-mail addresses: harazono@nihs.go.jp (A. Harazono), nana@nihs.go.jp (N. Kawasaki).

1570-0232/$ – see front matter © 2008 Elsevier B.V. All rights reserved.
doi:10.1016/j.jchromb.2008.05.006

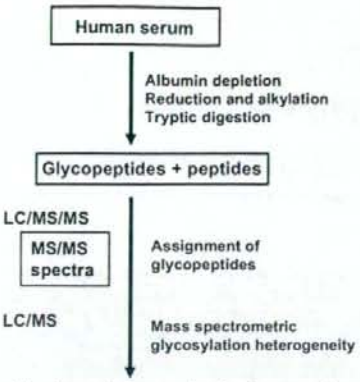

Fig. 1. Strategy for glycosylation analysis of abundant glycoproteins in serum. Human serum in which albumin was roughly removed was reduced and alkylated at cysteine residues. A mixture of peptides resulting from trypsin digestion was subjected to LC/MS/MS and LC/MS. Glycopeptides were assigned by elucidating MS/MS spectra (database searching). Mass spectrometric heterogeneity at each glycosylation site was analyzed by an additional LC/MS.

Recent progress in MS/MS and multiple-stage MS (MS^n) of glycopeptides allows for the characterization of both peptide and oligosaccharide moieties based on fragment ions [17,20–27]. Previously it was demonstrated that the Qq-TOF type mass spectrometer provides highly abundant carbohydrate-related ions at lower *m/z* values such as *m/z* 204 $[HexNAc+H]^+$ and 366 $[HexHexNAc+H]^+$, glycopeptide-related ions with sequentially lost saccharide units, including $[peptide+H]^+$ and $[peptide+GlcNAc+H]^+$ at higher *m/z* values, and *b*- and *y*-ions derived from peptide backbone [20,23,26,28]. These fragment ions could be used in database search to deduce peptide of glycopeptide.

In this study we demonstrated LC/MS(/MS) of human serum digest for the simultaneous glycosylation analysis of abundant serum proteins. Fig. 1 shows the strategy for the glycosylation analysis. Human serum, the albumin of which was depleted, was carboxymethylated and digested with trypsin. LC/MS/MS of the digest was performed by using the LC/Qq-TOF MS instrument. Glycopeptide ions were basically assigned by database searching with modified peak-list text files. Mass spectrometric heterogeneity at each glycosylation site was analyzed by an additional LC/MS, in which the acquisition of MS/MS was not allowed. By LC/MS of albumin-depleted human serum digest, we were successful in the site-specific glycosylation analysis of abundant serum glycoproteins.

2. Experimental

2.1. Materials

Pooled normal human serum was purchased from Sigma (St. Louis, MO, USA). Human haptoglobin and polyclonal immunoglobulin G, which were purified from normal human serum, were purchased from Calbiochem (San Diego, CA, USA). Modified trypsin was purchased from Promega (Madison, WI, USA). The water used was obtained from a Milli-Q water system (Millipore, Bedford, MA). All other reagents were of the highest quality available.

2.2. Sample preparation

Human serum (5 μl) was depleted of albumin using the Montage Albumin Depletion Kit (Millipore, Bedford, MA, USA) according to the manufacturer's protocol. Lyophilized albumin-depleted sample and each of the glycoproteins (100 μg) were dissolved in 50 μl of 0.5 M Tris–HCl buffer (pH 8.5) that contained 7 M guanidine hydrochloride and 5 mM EDTA. After the addition of 2 μl of 1 M dithiothreitol, the mixture was incubated for 30 min at 56 °C. Then, 4.7 μl of 1 M sodium monoiodoacetate was added, and the resulting mixture was incubated for 30 min at room temperature in the dark. The reaction mixture was applied to a PD-10 column (GE Healthcare, Little Chalfont, UK) to remove the reagents, and a fraction of the carboxymethylated proteins was dried. The sample was redissolved in 50 μl of 50 mM Tris–HCl buffer (pH 8.0). An aliquot of 1 μl of modified trypsin prepared as 1 μg/μl was added, and then the mixtures were incubated for 12 h at 37 °C. The enzyme digestions were stopped by boiling for 10 min and stored at −20 °C before analysis.

2.3. LC/MS and LC/MS/MS

The tryptic digests corresponding to 0.01–0.3 μl of human serum or a tryptic digest of purified commercially available glycoprotein (0.1–1.0 μg) was loaded onto a nanotrap (AMR Inc., Tokyo, Japan). After a wash with 10 μl of 2% (v/v) acetonitrile containing 0.1% (v/v) TFA, the trapping column was switched into line with the column. HPLC was performed on a Paradigm MS 4 (Michrome BioResources, Auburn, CA, USA) equipped with a MonoCap High Resolution 750 column (0.2 mm × 750 mm, GL Sciences Inc., Tokyo, Japan) at a flow rate of about 2 μl/min. The eluents consisted of water containing 2% (v/v) acetonitrile and 0.1% (v/v) formic acid (pump A) and 90% acetonitrile and 0.1% formic acid (pump B). Samples were eluted with 5% of B for 2.5 or 5.0 min followed by a linear gradient from 5 to 90% of pump B in 85 min or by linear gradients from 5 to 25% for 80 min, 25–45% for the next 60 min, 45–65% for the next 40 min and 60–90% for the next 20 min (total 205 min).

Mass spectrometric analyses were performed using a QSTAR Pulsar i Qq-TOF mass spectrometer (AB/MDS Sciex, Toronto, Canada) equipped with a nano-electrospray ion source. The mass spectrometer was operated in positive ion mode. The nano-spray voltage was set at 1700 V. Mass spectra were acquired over *m/z* 1000–2000 for MS, and *m/z* 100–2000 for MS/MS. After every regular MS acquisition, MS/MS acquisitions were performed against the top two multiply charged ions by a data-dependent acquiring method. The precursor ions with the same *m/z* as previously acquired were excluded for 60 or 90 s. The collision energy was varied between 30 and 70 eV depending on the size and charge of the molecular ion. The accumulation time of the spectra was 1.0 s for MS, and 2.0 or 5.0 s for MS/MS. All signals were monoisotopically resolved.

2.4. Assignment of glycopeptide peaks by database search

Detection and assignment of glycopeptide ions from LC/ESI MS/MS data were performed by elucidating MS/MS spectra or database search. Briefly, glycopeptide ions were selected manually based on presence of oligosaccharide oxonium ions such as *m/z* 204 and 366 in their MS/MS spectra. The information of *m/z* values and charge states of peptides in the glycopeptides was deduced by sequential degradation pattern at N-glycan core structure in their MS/MS spectra. The MS/MS spectra of glycopeptides were converted to peak-list text files, and then oligosaccharide-related ions (*m/z* 168, 186, 204, 274, 292 and 366 or ions under *m/z* 370)

and the ions larger than peptide ion were deleted. Modified peak-list text files were submitted to against the nonredundant human Swiss-Prot protein database (version 48.2) using Mascot search engine with following parameters: a specified trypsin enzymatic cleavage with two possible missed cleavage, peptide tolerance of 1.2 Da, fragment ion tolerance of 0.8 Da, and variable modifications of cysteine (carboxymethylation) or cystein (carboxymethylation) and methionine (oxidation). Suggested peptides were validated by manual inspection of the spectra, and the presence of more than four consecutive fragments of amino acid sequence was used as criteria for peptide identification.

3. Results

3.1. Locating glycopeptides in the chromatogram

Mass spectrometric glycosylation analysis of human serum was performed by LC/Qq-TOF MS of tryptic digest using in a positive ion mode. In this method, all serum glycoproteins should be completely digested by trypsin. When the tryptic digest was subject to LC/MS/MS with the MS range m/z 400–2000, results of Mascot database search using 3 missed cleavage sites suggested that most peptides were completely digested (missed cleavage <1) and few incompletely digested peptides (missed cleavage 3) were present. Many missed cleavage sites were present at N- or C-terminal, or adjacent to two or more acidic amino acid residues (D, E or carboxymethylated C) (data not shown). Fig. 2A shows the total ion chromatogram (TIC) obtained by LC/MS/MS with MS range m/z 1000–2000 of tryptic digest (corresponding to approximately 0.3 μl of serum) using a reversed phase MonoCap High Resolution 750 column (0.2 mm × 750 mm) with a gradient of 5–90% of B in 205 min. In order to locate the glycopeptide peaks and determine m/z and charge state, the intensity of the oxonium HexNAc$^+$ (m/z 204.05–204.15) that arose by data-dependent MS/MS was depicted as the extracted ion chromatogram (Fig. 2B). We confirmed that most of these MS/MS spectra were of glycopeptides by the presence of abundant carbohydrate-derived ions, such as m/z 204 ([HexNAc+H]$^+$), 186 ([HexNAc+H−H_2O]$^+$), 292 ([NeuAc+H]$^+$), 274 ([NeuAc+H−H_2O]$^+$) and 366 ([HexHexNAc+H]$^+$).

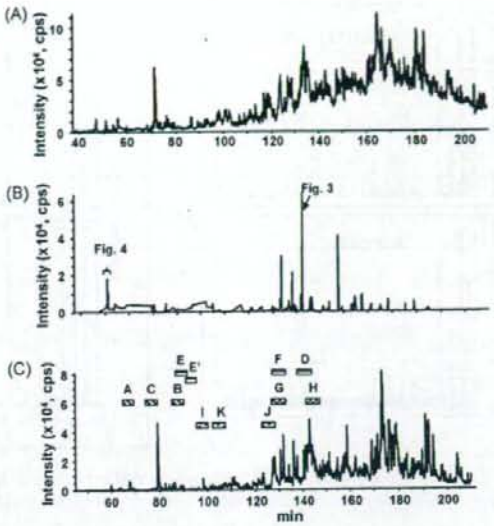

Fig. 2. LC/MS/MS and LC/MS of tryptic digest of human serum. (A) TIC (m/z 1000–2000) obtained by the LC/MS/MS. (B) EIC (m/z 204.05–204.15) obtained by the data-dependent MS/MS. (C) TIC obtained by the additional LC/MS in which data-dependent MS/MS was not allowed. Peak assignment: A, IgG1; B, IgG2; C, IgG3/IgG4; D–F, haptoglobin; G and H, transferrin; I–K, ceruloplasmin. Mass spectra of fractions A–K are shown in Fig. 7.

3.2. Assignment of glycopeptide peaks by a database search

Glycopeptides were assigned by manual database searching. As a representative example, the MS/MS spectrum acquired from [M+4H]$^{4+}$ (m/z 1221.8 (4+)) at 133 min is shown in Fig. 3. There are some abundant ions derived from carbohydrates, such as m/z 204, 186, 292, 274 and 366 in the lower m/z region. Degradation pattern and mass difference of 203 u between the fragment ions at m/z 1340.2 (2+) and those at 1441.7 (2+) in the higher m/z region suggests that the ions are [peptide+2H]$^{2+}$ and [peptide+HexNAc+2H]$^{2+}$, respectively. Based on these m/z values the molecular mass of

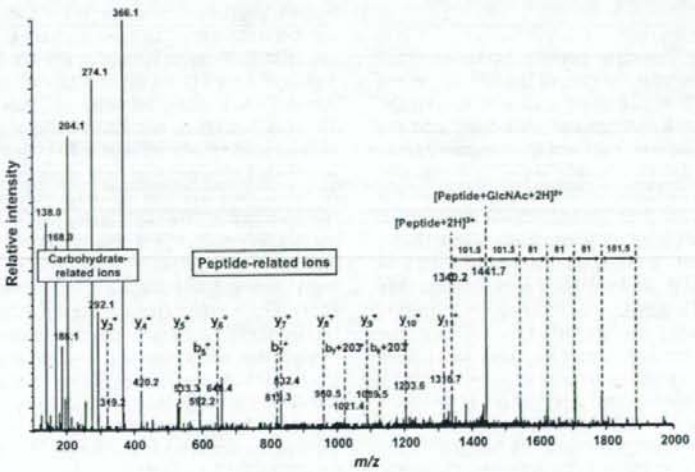

Fig. 3. MS/MS spectrum acquired from m/z 1221.8 (4+) by data-dependent LC/MS/MS of trypsin-digested human serum. Mascot database search using m/z 1340.2 (2+) of peptide and fragment ions (m/z 370–1300) suggested peptide sequence MVSHHN^{184}LTTGATLINEQWLLTTAK in haptoglobin (P00738).